UNIVERSIDAD DE INVESTIGACIÓN DE TECNOLOGÍA EXPERIMENTAL YACHAY

Escuela de Ciencias Biológicas e Ingeniería

TÍTULO: Ultrasound-mediated synthesis of Quantum Dots: A comparative review and potential outlooks in biomedicine

Trabajo de integración curricular presentado como requisito para la obtención del título de Ingeniero Biomédico

Autor:

Estrada Toro Javier Eduardo

Tutor:

PhD – Nelson Santiago Vispo

Cotutor:

PhD – Si Amar Dahoumane

SECRETARÍA GENERAL
(Vicerrectorado Académico/Cancillería)
ESCUELA DE CIENCIAS BIOLÓGICAS E INGENIERÍA
CARRERA DE BIOMEDICINA
ACTA DE DEFENSA No. UITEY-BIO-2021-00034-AD

A los 29 días del mes de noviembre de 2021, a las 11:30 horas, de manera virtual mediante videoconferencia, y ante el Tribunal Calificador, integrado por los docentes:

Presidente Tribunal de Defensa	Dr. CHACON TORRES, JULIO CESAR , Ph.D.
Miembro No Tutor	Dr. ALEXIS FRANK , Ph.D.
Tutor	Dr. SANTIAGO VISPO, NELSON FRANCISCO , Ph.D.

El(la) señor(ita) estudiante **ESTRADA TORO, JAVIER EDUARDO**, con cédula de identidad No. **1715068886**, de la **ESCUELA DE CIENCIAS BIOLÓGICAS E INGENIERÍA**, de la Carrera de **BIOMEDICINA**, aprobada por el Consejo de Educación Superior (CES), mediante Resolución **RPC-SO-43-No.496-2014**, realiza a través de videoconferencia, la sustentación de su trabajo de titulación denominado: **Ultrasound-mediated synthesis of Quantum Dots: A comparative review and potential outlooks in biomedicine** , previa a la obtención del título de **INGENIERO/A BIOMÉDICO/A**.

El citado trabajo de titulación, fue debidamente aprobado por el(los) docente(s):

Tutor	Dr. SANTIAGO VISPO, NELSON FRANCISCO , Ph.D.

Y recibió las observaciones de los otros miembros del Tribunal Calificador, las mismas que han sido incorporadas por el(la) estudiante.

Previamente cumplidos los requisitos legales y reglamentarios, el trabajo de titulación fue sustentado por el(la) estudiante y examinado por los miembros del Tribunal Calificador. Escuchada la sustentación del trabajo de titulación a través de videoconferencia, que integró la exposición de el(la) estudiante sobre el contenido de la misma y las preguntas formuladas por los miembros del Tribunal, se califica la sustentación del trabajo de titulación con las siguientes calificaciones:

Tipo	Docente	Calificación
Presidente Tribunal De Defensa	Dr. CHACON TORRES, JULIO CESAR , Ph.D.	10,0
Tutor	Dr. SANTIAGO VISPO, NELSON FRANCISCO , Ph.D.	10,0
Miembro Tribunal De Defensa	Dr. ALEXIS FRANK , Ph.D.	10,0

Lo que da un promedio de: **10 (Diez punto Cero)**, sobre 10 (diez), equivalente a: **APROBADO**

Para constancia de lo actuado, firman los miembros del Tribunal Calificador, el/la estudiante y el/la secretario ad-hoc.

Certifico que *en cumplimiento del Decreto Ejecutivo 1017 de 16 de marzo de 2020, la defensa de trabajo de titulación (o examen de grado modalidad teórico práctica) se realizó vía virtual, por lo que las firmas de los miembros del Tribunal de Defensa de Grado, constan en forma digital.*

ESTRADA TORO, JAVIER EDUARDO
Estudiante

Dr. CHACON TORRES, JULIO CESAR , Ph.D.
Presidente Tribunal de Defensa

Dr. SANTIAGO VISPO, NELSON FRANCISCO , Ph.D.
Tutor

Dr. ALEXIS FRANK , Ph.D.
Miembro No Tutor

ALARCON FELIX, KARLA ESTEFANIA
Secretario Ad-hoc

AUTORÍA

Yo, JAVIER EDUARDO ESTRADA TORO, con cédula de identidad 1715068886, declaro que las ideas, juicios, valoraciones, interpretaciones, consultas bibliográficas, definiciones y conceptualizaciones expuestas en el presente trabajo; así cómo, los procedimientos y herramientas utilizadas en la investigación, son de absoluta responsabilidad de el/la autora (a) del trabajo de integración curricular. Así mismo, me acojo a los reglamentos internos de la Universidad de Investigación de Tecnología Experimental Yachay.

Urcuquí, diciembre 2021.

_____

Javier Eduardo Estrada Toro
CI: 1715068886

AUTORIZACIÓN DE PUBLICACIÓN

Yo, JAVIER EDUARDO ESTRADA TORO, con cédula de identidad 1715068886, cedo a la Universidad de Tecnología Experimental Yachay, los derechos de publicación de la presente obra, sin que deba haber un reconocimiento económico por este concepto. Declaro además que el texto del presente trabajo de titulación no podrá ser cedido a ninguna empresa editorial para su publicación u otros fines, sin contar previamente con la autorización escrita de la Universidad.
Asimismo, autorizo a la Universidad que realice la digitalización y publicación de este trabajo de integración curricular en el repositorio virtual, de conformidad a lo dispuesto en el Art. 144 de la Ley Orgánica de Educación Superior

Urcuquí, diciembre 2021.

_____

Javier Eduardo Estrada Toro
CI: 1715068886

Resumen

Los Quantum Dots (QD) son un grupo diverso de nanomateriales semiconductores que han ganado un interés creciente en una gran diversidad de campos debido a sus capacidades únicas, así como a sus excepcionales propiedades ópticas y tamaño. Se han desarrollado muchos métodos para sintetizar QD, incluidos los enfoques basados en ultrasonidos (también llamados metodos basados en sonoquímica). El ultrasonido se ha empleado para sintetizar muchos nanomateriales además de los QD, como nanobarras, nanoplacas y nanoestructuras complejas. En comparación con otros métodos de síntesis de QD, los enfoques basados en ultrasonidos proporcionan una alternativa ecológica, más simple, rápida, segura y accesible que otros métodos. En esta revisión, destacaremos la diversidad de los QDs, sus aplicaciones y las deficiencias actuales. También discutiremos las propiedades físicas y químicas del ultrasonido, sus efectos de varios parámetros experimentales sobre los precursores de nanomateriales, sus ventajas y limitaciones, y las características de un aparato de ultrasonido simple. Finalmente, esta revisión incluye un resumen y una comparación de varios métodos de síntesis de QDs para dos tipos prevalentes de QDs. Con base en parámetros experimentales establecidos, discutimos el potencial y la relevancia del ultrasonido en el contexto de los procesos de síntesis de QDs.

Palabras clave: Quantum Dots, nanosintesis, ultrasonidos.

Abstract

Quantum Dots (QDs) are a diverse group of semiconductor nanomaterials that have gained increasing interest in a great diversity of fields due to their unique capabilities, as their outstanding optical properties and size. Many methods have been developed to synthesize QDs, including ultrasound-based (also referred to as sonochemistry-based) approaches. Ultrasound has been employed to synthesize many nanomaterials aside from QDs, such as nanorods, nanoplates, and complex nanostructures. Compared to other QD synthesis methods, ultrasound-based approaches provide a simpler, faster, safer, and more accessible green alternative than other methods. In this review, we will highlight the diversity of QDs, their applications, and current shortcomings. We will also discuss the physical and chemical properties of ultrasound, its effects of various experimental parameters on nanomaterial precursors, its advantages and limitations, and the characteristics of a simple ultrasound apparatus. Finally, this review includes a summary and comparison of several QD synthesis methods for two prevalent QD types. Based on established experimental parameters, we discuss the potential and relevance of ultrasound within the context of QD synthesis processes.

Keywords: Quantum Dots, nanoparticles, ultrasounds.

Table of Contents

List of Figures

List of Tables

Chapter I

Introduction

Initially described in 1981 by Ekimov and Onushenko (1), Quantum Dots (QDs) were initially believed to be among the first semiconductors with a three-dimensional structure. They highlighted the size effects that these structures possessed. The term "quantum dot" was first used in 1988 by Reed (2) to refer to structures that they synthesized with some unique characteristics: they had quantum confinement to zero dimensions concerning the quantum confinement effect, which relates to nanocrystals with a smaller size than the Bohr radius have a determined amount of energy-related to their size (3).

With those characteristics, QDs were sometimes referred to as "artificial atoms" and were initially synthesized in semiconductor crystals or glass matrixes, in which they appeared individually 0.3 to 0.4 nm apart from each other (4). Although the term "artificial atom" was somewhat expected, it was understood that each QD or artificial atom contained various electrons within the matrix structure, implying that several real atoms comprised one artificial atom in a crystal matrix. These atoms did not get trapped within the atoms that make up the crystal and are only attached to the QD's potential is explained by the quantum-mechanical theory of solids. This theory states that some electrons behave as free electrons when they are part of a crystal structure, only differing by their mass (4,5).

One of the most prevalent methods for synthesizing QDs and nanomaterials involves the ultrasonic irradiation of materials. As we will analyze in later sections, ultrasound has unique characteristics that make it an extremely versatile tool for QD synthesis. With such a wide variety of QD compounds and synthesizing methods, many of these methods are becoming cheaper, more accessible, and more efficient; ultrasound remains an irreplaceable tool within this field. This review aims to summarize some of the most important synthesis methods for QD fabrication, compare them, and provide a relevant bibliographic context of the importance of ultrasound methods within the rapidly expanding QD synthesis field.

Chapter II

Problem statement

Quantum Dots encompass a large group of nanomaterials with a wide range of applications depending on their characteristics, especially within the biomedical field. The size and the specific nanostructures of Quantum Dots often pose a challenge in their synthesis process, with many methods being developed and improved during the past few decades. Ultrasounds are used in many of these methods to synthesize Quantum Dots, either directly or assisting other processes. They offer unique conditions for the formation of these nanomaterials and are particularly easy to use and affordable. With the rapid discovery of new Quantum Dots, configurations, and processes, there is often a moderate difficulty in finding updated literature that can serve as a starting point for studies attempting to synthesize Quantum Dots of specific precursors and characteristics with a limited budget, something ultrasound-based methods excel at.

Since new Quantum Dots are being discovered continuously and novel ultrasound applications for their synthesis, a comparative study that explores the potential of ultrasound methods for more complex and novel Quantum Dot configurations could prove to be of outstanding academic relevance.

Objective

To prepare a literature review that summarizes the main factors in ultrasound-based synthesis approaches for QDs and explores through comparisons the prospects of these approaches to serve as a starting point for future studies.

Specific Objectives

i.   To highlight the diversity in types of QDs, summarize their properties and applications (both in and out of the biomedicine field).

ii.   To introduce the diversity and categorization of QD synthesis methods for various applications, the pros and cons, and their specific applications.

iii.   To summarize the relevance of ultrasound-based approaches as synthesis methods for nanomaterials' general field even when newer techniques are available and highlight the unique capabilities of this method.

iv.   Integrate the information summarized and introduced in previous sections to show the relevance, potential, and most pressing limitations of QD synthesis through ultrasound-assisted approaches.

Chapter III

Quantum Dot diversity, properties and applications

Quantum Dots by elemental group association

QDs can be very diverse, from their composition, which consists of elements of the periodic table corresponding to the groups II-IV or III-V, as well as their size, which, as cited previously, is smaller than the Bohr radius of the exciton at a range of 4 to 12 nm in diameter (6,7). Despite this distinction, there has been some historical discussion on whether QDs should be considered from sizes in the range of 2-20nm(8) or strictly below 10nm(9). For this reason, there are many ways to classify QDs, and in this review, we will be using their classification according to their chemical composition, major groups derived from other types of nanomaterials, and groups that are not directly tied to a single chemical group.

In regards to their chemical composition, QDs are classified in 12 categories: HgS (10), HgSe (11), HgTe (12), CdS (13), CdSe (14), CdTe (14), ZnO (15), ZnS (16), ZnSe (17), ZnTe (18) QDs are type II B-IV A QDs (19). These types of QDs are part of another type of classification known as semiconductor Quantum Dots, which have a broad array of applications in the biomedical (20), sensing (21), and imaging fields (22). Type II B-IV A QDs have a highly tunable fluorescence emission that makes them highly suitable for these applications (23). However, one downside of these QDs (specifically semiconductor QDs) is their biotoxicity and solubility, which limit their safety, therefore limiting their in vivo uses.

Type III A-V A QDs is another extensive group characterized for having remarkably stable optical properties thanks to having predominantly covalent bonds within their structures, especially when compared to type II B-IV A QDs (19). The main downside of this type of QDs is their low quantum yield, a measurement of photon emission defined by the ratio of photons absorbed vs. photons emitted (24,25). To minimize this problem, the QDs in this category are often coated with elements that have wider energy gaps as in InP/ZnS QDs (being InP one of the most commonly used QDs within this category) (26).

Type IV A-VI A QDs include PbS (27), PbSe (28), and PbTe (29), which all have narrower energy gaps which cause their fluorescent emission region to be located in the near

and mid-infrared spectral ranges. These characteristics make this type of QDs beneficial for solar cell applications to absorb the most visible light. They can generate multiple charge-carrier pairs from a single optical stimulation, a process known as multiple-exciton generation(30).

Another remarkable and widely applicable category is type IV A QDs which possess high biocompatibility and safety while maintaining intense photoluminescence in solution and solids via surface passivation(31). In this group, we can find Si (32), Graphene (33), and Carbon QDs (CQDs). CQDs are particularly notorious for their physicochemical properties, outstanding biocompatibility, and fluorescence.

Black Phosphorous QDs (BPQDs) have a similar composition to type IV A QDs but differ in enough aspects to be classified in their category, type V A (34). BPQDs have auspicious properties that have demonstrated a possible application as a phototherapy agent for cancer treatment, although limited by its high reactivity with oxygen and water, leading to rapid degradation during in-vivo circulation (35). BPQDs also have nonlinear optical properties that have allowed for recent significant advancements in ultrafast laser technology for photonic therapy use and imaging(36,37). Graphene-based composites have in turn been used widely across many fields, but their unique properties have impacted the field of optics by far more than any others(38,39).

Type I B-III A-VI A QDs is a ternary group known for mostly having adjustable bandgaps. In this group, we find $CuInS_2$, $CuInSe_2$, and $AgInS_2$ QDs, and each one's fluorescence can be adjusted continually within the red to the near-infrared region(40).

There are also Cu_2S QDs which are classified in their category (I B-VI A), which are employed in the solar cell industry (41) and in novel biomedical uses such as the recently proposed inhibition of protein fibrillation to treat degenerative diseases(42).

Quantum Dots by structural association

As many previous examples have already demonstrated, the unique and versatile optical properties of QDs are the main reason they are widely present and applied in so many different fields nowadays. Thus far, the types of QDs detailed are primarily relevant in biomedical imaging, biosensing, and solar cell fabrication through photovoltaic devices (12,43–45). QDs

can be integrated into core/shell structures which can accentuate some of their properties or alleviate their shortcomings, allowing for an even broader and deeper field of applications (46).

Among these composite QDs, we have Polymer Dots (commonly known as Pdots), a type of semiconductor nanoparticle similar in size to semiconductor QDs, while offering some advantages such as a fast conversion rate of radiation emission, high brightness, and stability. These properties make Pdots very viable for cancer treatment, where various tumor-targeting methods have been proposed and demonstrated(47–49) and bioimaging(50–53).

Another versatile type of QDs is transition metal dichalcogenide (TMDC) QDs. These QDs are characterized by having a remarkably high quantum yield and the ability to be functionalized with ease. These QDs are mainly based on Titanium and Molybdenum elements, with one example being MoS_2 QDs which is used as a catalyst for oxygen evolution reactions (54). MoS_2 QDs are also commonly used in biosensors (55) and oncology (56) due to their ability to enhance photoacoustic imaging, X-ray imaging, and computed tomography, signaling a higher efficiency when performing radiotherapy in cancer patients.

Another rapidly gaining relevance is MXene dots based on MXene sheets(57), synthesized by etching selective layers of *sp* elements from a corresponding three-dimensional MAX phase(57). An MXene three-dimensional phase consists of 3 essential elements summarized in the formula $M_{n+1}AX_n$, where M A and X represent: M as an early *d*-block transition metal; X is a Carbon and either or both Nitrogen; n can be (n=1, 2, 3); A can be F−, O2− and OH− or any main-group *sp* element (although the ones applied on this field the most are predominantly from groups IIIA or IVA) (58,59). More than 70 MAX three-dimensional phases are identified in the relevant literature, but only around 11 of there are currently employed in elaborating MXene sheets. At the moment, only these are considered members of the MXene family, although it is a very novel group and is expected to proliferate throughout the next few years (58,60–66). MXene sheets are often referred to as graphene analogs as they share some properties due to their 2D nature(67). MXene materials have high metallic conductivity, hydrophilicity, and biocompatibility(66); properties that they share with their MXene QD counterparts. The advantages of MXene QDs come from their fluorescence and ultra-small size properties that expand the use of these materials in various fields such as oncology(68), biomedicine(69), optics(70,71), and bioimaging(72).

Another QD type that has seen widespread implementation in multiple industries is inorganic perovskite QDs (IPQDs), which are used in the manufacturing of light-emitting diodes (LED) (73), QD-based lasers(74), light sensors(75), and solar cells(76).

As we have seen from the QD types detailed in this section, each type can have unique properties applicable in specific instances. In many cases, various types of QDs can overlap with other types within the same field. Most QD types we have detailed are employed in solar cell manufacturing, cancer phototherapy, and biomedical imaging, with each one having pros and cons that allow for more situational uses. Another thing to consider is that the vast majority of quantum dots need to be integrated into some form with other elements for practical applications. This is usually done by doping the QDs surface with said elements (the proposed degenerative treatment based on Cu_2S QDs has the QDs doped with Zn (42), for example) or integrating them into nanocrystals or core/shell structures (ZnSe QDs acquired modified in-vivo capabilities such as water solubility when coupled with an InAs shell(43)).

Out of all the fields mentioned, biomedicine is usually regarded as the most relevant for QD use in humans. Aside from the applications above, QDs are highly effective drug delivery and targeting agents as labels and probes. It is worth emphasizing the origin of these nanostructures' unique properties that have made them often irreplaceable in these fields, mainly their optical capabilities. The optical capabilities of QDs originate from their inorganic core, which is commonly modulated after its activation through an inorganic shell and sometimes ligands that are bound to the shell. All these components are also the factors that allow QDs to be so versatile, as each one of these three components can be modified in elemental composition, structure, and size. Adjusting each of these factors produces a wide array of possible QDs with narrow emission or broad absorption spectra and custom light emission. Modification of these factors can also result in QDs with high fluorescence quantum yields that maximize their efficiency, high durability due to photochemical robustness, reduction or increase in fluorescence intermittency, broad stokes shift, and resistance to photo bleach effect, which also makes them reliable dyeing agents(77).

QUANTUM DOT SYNTHESIS APPROACHES

QD Synthesis methods by the state of precursors

Synthesis methods of QDs can be classified by two different metrics, which are universal for all types of nanomaterials. The first one is based on the state of the precursor of the desired QDs. If we are starting from bulk materials and then developing the smaller architectural structures, then it is called a "top-down" method; if, on the contrary, we begin with the smaller atomic or molecular components to build the relatively more significant nanostructures, then it is called a "bottom-up" method(78).

"Top-down" approaches

"Top-down" approaches within the field of nanomaterial synthesis are, for the most part, considered extensions of pre-existing methods employed to produce micron-sized particles. For this reason, these methods are intrinsically more straightforward as they involve the division and predominantly physical approached to achieve the desired nanoparticles. The simplistic nature and extensive history of methods like lithographic processes have been widely used in the semiconductor industry for decades(79) and in some early production of QDs(80). Some of these processes, specifical photolithography, have been used to pattern via electron abrasion the desired structures, with their main disadvantage being the imperfections produced. These imperfections accentuate when developing more minor features due to the medium's optical limitations (81).

"Bottom-up" approaches

"Bottom-up" approaches are very prevalent in nanotechnology literature. These types of approaches have also been quite common in industrial applications of nanomaterials even a century ago. This is because bottom-up approaches encompass the synthesis of materials via crystal growth, and crystal growth methods involve the assembly of atoms and molecules into determined crystalline structures. The bottom-up approach's advantages are the more homogeneous assembly and chemical composition, and fewer defects are usually expected. They are also generally less expensive to use and more suitable for mass production. Some examples of bottom-up approaches are gas-based reduction and colloidal dispersion.

13

A critical difference between these two types of approaches is that nanostructures' assembly mainly involves self-assembly of the precursors driven by reducing Gibbs free energy in the bottom-up methods. Top-down approaches mainly involve introducing internal stresses to bulk materials and other elements that might act as contaminants.

Hybrid approaches

While some methods described so far fall strictly within these categories, some others might play a part in different synthesis stages that might involve both top-down and bottom-up approaches and are known as hybrid approaches.

QD Synthesis methods by chemical reaction involvement

The mere existence of hybrid approaches is why we might find it helpful to be able also to classify all "top-down" and "bottom-up" nanomaterial synthesis methods by another measurement. Another categorization based on the nature of the process and the involvement of chemical reactions is subdivided into physical and chemical approaches.

Physical Methods

We first have physical methods characterized by the lack of chemical reactions or interventions in the process. Physical methods mainly involve nucleation and particle growth within solutions, or sometimes in vapor phases. Within the context of QD synthesis, the only purely physical method with relevance for practical purposes is molecular beam epitaxy(82). This method has been employed for decades, not only for the synthesis of nanomaterials but also for a wide array of semiconductors, metals, and oxides(83). It involves the deposition with beams of atomic or molecular sources on substrates with a crystalline structure, usually atomically smooth and placed in a vacuum. When used for QD synthesis, it induces an ordered QD array's spontaneous formation on the crystalline structures' surface. This spontaneous formation is generated by the mismatch between the lattice constants on the surface of the epitaxial films, and the resulting dispersion of the QDs causes a stress reduction in the film. The particular method detailed here has been used in the past to produce extremely small dispersions of the size distribution function (with a 2% difference across all QDs produced, a record low at the time) on PbSe QDs(84). The main downside pointed out in the study about the molecular beam epitaxy method was the requirement for specialized and expensive equipment and

materials with remarkably high purity. Since this method involves introducing more minor elements to self-assemble into more complex structures, this specific method is a "bottom-up approach". Nonetheless, most physical methods are also classified as "top-down" methods. Among the most well-known methods are lithographic approaches - which include electron lithography and photolithography - used for decades to fabricate microelectronic components for the semiconductor industry.

Chemical methods

In contrast to physical methods, nanomaterials' chemical synthesis methods involve chemical reactions that induce the chemical transformation of matter. In this category, most methods represent liquid-phase condensation or a chemical reaction that results in a supersaturation that allows for the nanoparticles' nucleation and formation. For this reason, most chemical methods also fall in the "bottom-up" category. One of the first successful methods to synthesize QDs two decades ago was through organometallic synthesis, a "bottom-up," three-step process. While placed in an organic solvent at high temperatures, the precursor materials undergo nucleation, growth, and termination; through the manipulation of reaction conditions, this method allows for the precise adjustment of the size (and therefore the emission wavelengths) of the QDs. Many QD varieties have been synthesized through organometallic routes, with some examples being PbS QDs(85) and CdTe/CdS QDs(86). The most important parts of the processes involving QD synthesis occur in the post-synthesis treatment since a significant portion of QDs have a meager quantum yield of luminescence when they are initially produced. Physical methods are usually involved in these post-synthetic treatment phases, where QDs usually acquire their characteristic efficient luminescence and gain most of their utility(87).

Biological methods

Some literature considers QD synthesis methods that involve living organisms as their separate category from physical or chemical methods. In a similar fashion to chemical approaches, most biological-mediated nanomaterial synthesis methods are classified as "bottom-up" approaches. Although less prevalent than the two methods previously described, biological methods offer unique advantages that deserve to be mention, especially when trying to develop QDs or nanomaterials intended for biomedical purposes. Physical methods often

offer less stable nanostructures, and the irregularities that stem from these processes can cause potential threats to humans. Chemical methods, in many instances, involve the use of toxic chemicals (or non-polar solvents, which can also be problematic in biological interactions) to synthesize nanoparticles can also limit their clinical use(88). In this landscape, biological methods offer unique capabilities as they often offer a cost-effective, safe, sustainable, and environmentally friendly alternative to traditional methods. Some of the drawbacks of this type of approach include less control on the size distribution, crystallinity, and shape of the nanomaterials, and these methods can also be notoriously time-consuming.

Chapter IV

ULTRASOUNDS FOR NANOMATERIAL SYNTHESIS

The multi-step integration of different types of synthesis methods mentioned previously is even more relevant in some methods that can selectively be used either as a physical approach or a chemical approach (or even both simultaneously), as is the case with ultrasound-based approaches for the synthesis of nanomaterials.

The irradiation of materials with ultrasounds has had an essential focus in nanomaterial synthesis for more than two decades and has used both their physical and chemical effects for their production(89–91). The wide array of processes that ultrasounds can trigger position them as some of the most versatile tools in the fabrication of nanomaterials with various sizes, compositions, and structural architectures(92). In this section, we will identify and classify the chemical effects and physical effects of ultrasound-based methods.

Chemical effects of ultrasound

The mention of chemical effects might intuitively imply a direct chemical interaction of the soundwaves with the precursor materials' molecular species. Still, it refers to a series of interactions encompassed within a field called sonochemistry. In a liquid medium, sonochemistry manifests as the acoustic cavitation that forms bubbles in the medium, which collapse impulsively(93). These collapses occur when the bubbles reach specific sizes and become resonant to the frequency of the ultrasound irradiation introduced to the medium. The implosions caused by this resonance have been shown through spectroscopic studies to create clouds of cavitating bubbles with internal temperatures and pressures of 5000K and 1000 bar(93), with even higher values when isolated to single bubble cavitation(94–96). These extreme conditions cause chemical reactions within these regions and the reason why some approaches to ultrasound are labeled as sonochemical.
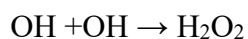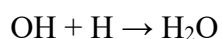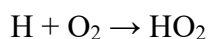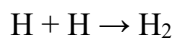
The local heating of targeted areas is high enough to dissociate all chemical bonds (even including N_2 bonds[97], which are more prone to dissociation at higher frequencies). When gases or any volatiles present within the imploding bubble react or maintain chemical alterations, we refer to this process as a *primary sonochemical reaction.* In contrast, *secondary sonochemical reactions* refer to the reactions that occur after the reactions in the extreme conditions caused by the imploding bubbles have already taken place. The resulting species have migrated to the surrounding liquid[98]. One thoroughly documented process occurs when water is the sonicated liquid, and it is the sonolysis of water[99,100]. As the name implies, this process involves separating water molecules into highly reactive hydrogen atoms and hydroxyl radicals. This separation takes place when bonds dissociate in the hot spot generated by the imploding bubbles. When the resulting atoms and molecules dissipate through diffusion from the hot spot, they undergo subsequent reactions that we have established as secondary sonochemical reactions and can include oxidations, reductions, hydroxylations of organics, among others.

Water sonolysis can be summarized as a series of rapid reactions involving both primary and secondary sonochemical reactions that involve both liquid and dissolved gases –such as O_2– and the resulting overall reactions are heavily dependant on the conditions. The reactions involved in this process are differentiated, as shown below.

Primary sonochemical reaction:

$$H2O \rightarrow (Ultrasound) \rightarrow H + OH$$

Secondary sonochemical reactions:

$$H + H \rightarrow H_2$$

$$H + O_2 \rightarrow HO_2$$

$$OH + H \rightarrow H_2O$$

$$OH + OH \rightarrow H_2O_2$$

It must be pointed out that these reactions correspond to the reactions involved in the ultrasound irradiation of aqueous solutions. Similar processes involving non-aqueous solutions produce radical species that can then be subjected to other processes compared to aqueous solution sonication, such as redox reactions, recombination, elimination reactions, and disproportionation reactions. These types of interactions will be analyzed further in the following subsections.

Primary sonochemistry for nanoparticle synthesis

One of the first reported successful syntheses of metal nanoparticles from volatile precursors involved using sonolysis, namely iron pentacarbonyl, to produce nearly pure amorphous iron(101). The method used in this report and every study produce sonolysis of volatile organometallic compounds that involve dissolving the compound in solvents with low vapor pressure, such as alkane solvents or ionic liquids(102–104), and then applying intense sonication. The resulting conditions caused by the interaction heavily favor the dissociation of metal-ligand bonds, allowing individual metal nanoparticles to form. The bubble implosion event is a very rapid phenomenon, and the extreme temperatures it generates also dissipate very quickly, causing a fast cooldown of the resulting nanoparticles. Since proper crystallization requires a determined amount of time, the quick dissipation of heat and pressure prevents an ordered crystallization from happening. The nanoparticles, therefore, appear as amorphous particles, coupled in agglomerations of 20nm particles. Some surfactants such as oleic acid can be added to obtain colloidal nanoparticles, as they can act as trapping agents for the particles formed during cavitation and the tail of the oleic acid stabilizes the colloids(105). A visualization of these interactions through transmission electron microscopy (TEM) can be seen in [Figure 1].
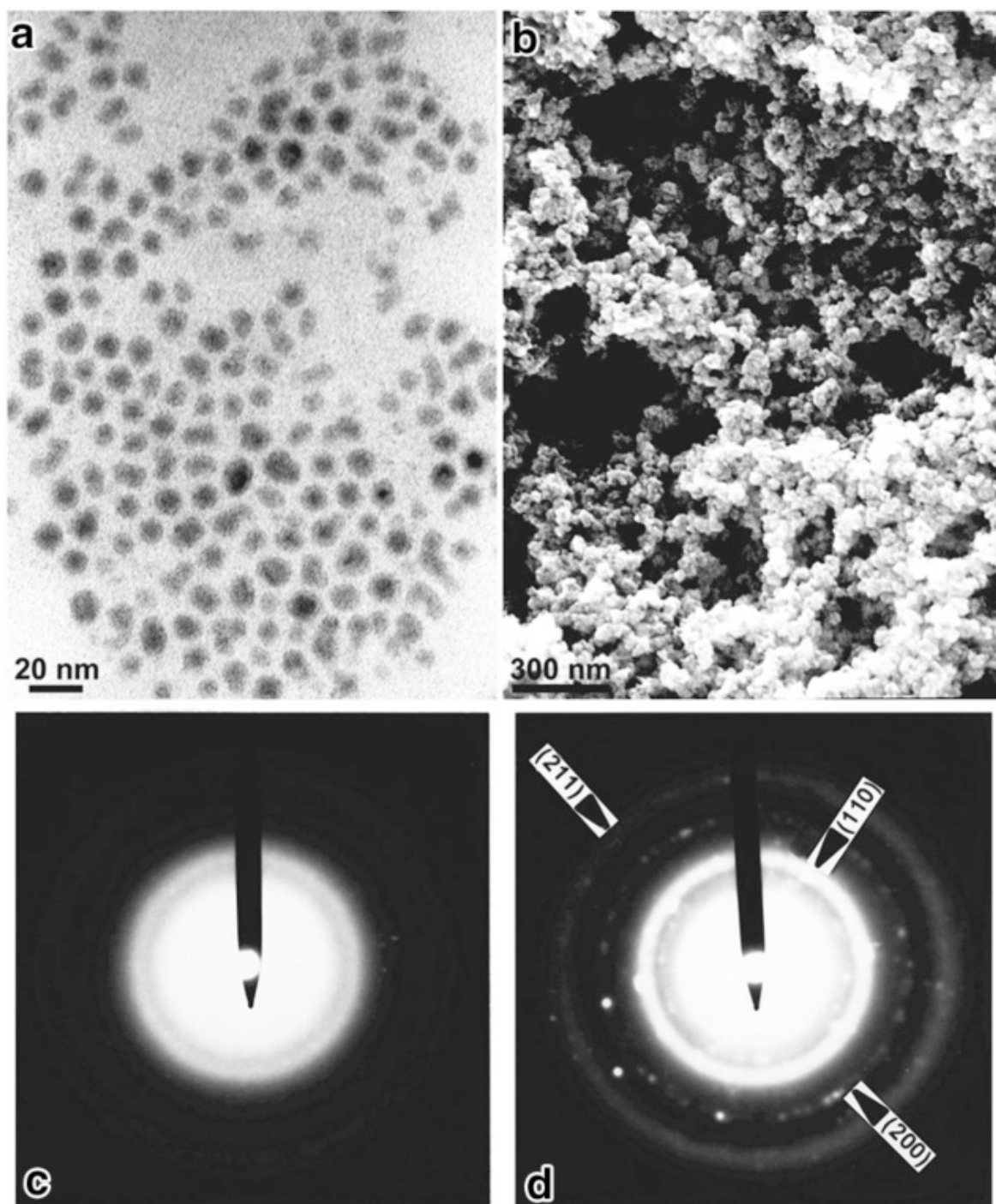
Figure 1.(a) Transmission electron micrograph of ultrasound-synthesized amorphous iron nanoparticles. (b) Scanning electron micrograph of agglomerated amorphous iron nanoparticles. (c) Electron diffraction pattern demonstrating the amorphous nature of the iron colloids. (d) Electron diffraction pattern showing the crystallization induced by heating from the electron beam. Reproduced with permission from Ref. (105).

Existing nanoparticles can also be used in the reaction process to serve as templates for the formation of sulfide and oxide nanoparticles. Template nanoparticles for these procedures are mainly carbon nanoparticles or silicon oxide (SiO_2) nanoparticles. In the presence of

carbon nanoparticles, the ultrasound-mediated synthesis of amorphous iron is altered, and the iron oxidizes rapidly upon contact with air, causing crystallization of the nanoparticles in a hollow formation(106). The study previously referenced repeated the same process without the involvement of carbon nanoparticles, and the result was that only amorphous iron oxide particles were synthesized.

Silica nanoparticles can also be used as templates to form other types of hollow nanoparticles. In order to form hollow MoS_2 particles, silica nanoparticles are placed in the same medium as Mo(CO)6 and are subsequently sonicated to produce the same phenomenon as in the previous example with carbon nanoparticles(107). In this instance, the template elements are not removed by combustion, but the silica is rather washed out with hydrofluoric acid. The referenced study also demonstrated the chemical advantages of hollow nanoparticles as a catalyst. The study showed an increased hydrodesulfurization catalytic activity of the hollow MoS_2 nanoparticles compared to non-hollow MoS_2 nanoparticles. The non-hollow MoS_2 nanoparticles were also produced through sonication but without silica nanoparticles present in the medium.

Hollow MoO_3 nanoparticles can also be produced through this method, substituting silicon nanoparticles with sulfur, and these particles could be annealed to form hollow nanocrystals.

Secondary sonochemistry for nanoparticle synthesis

As established previously, secondary sonochemistry deals with the molecular products produced by imploding cavitating bubbles from primary sonochemical processes. These processes are used to synthesize nanoparticles in the liquid phase and are extensively used methods in good part due to their ability to cause interactions with nonvolatile species. One of the earlier reports identifying the properties of secondary sonochemical reactions dates from three decades ago to produce colloidal gold(108). Colloidal gold is an important immunological marker for transmission electron micrographic studies. At the time of the study(108) the only process capable of producing this nanoparticle at a suitable small size for bioimaging at the ultrastructural level involved reducing the bulk of gold with phosphorous. Other reducing agents were used at the time, such as formaldehyde and ethyl alcohol, but they resulted in bigger particle sizes than phosphorous-based processes. The ultrasound process turned obsolete the previous methods as it could produce nanoparticles with diameters of 10nm without the need of extra precursors, as well as allowing for easier preparation

(improving the speed at which new batches could be produced) and a better dispersion of the gold colloids.

With a small amount of 1-propanol, another study performed the sonochemical reduction of Au(III) to produce Au nanoparticles at different frequencies(109). This study was set to describe the mechanical effects of cavitation on sonochemically synthesized gold nanoparticles and establish the relationship between the ultrasound frequency with the variation in size of the resulting nanoparticles and the variation of the reduction rate. In [Figure 2], we can see the variation of Au(III) reduction at different frequencies, starting with the lowest rate at 20 kHz, then the highest rate being obtained at 213 kHz, and then decreasing as the frequency increases.
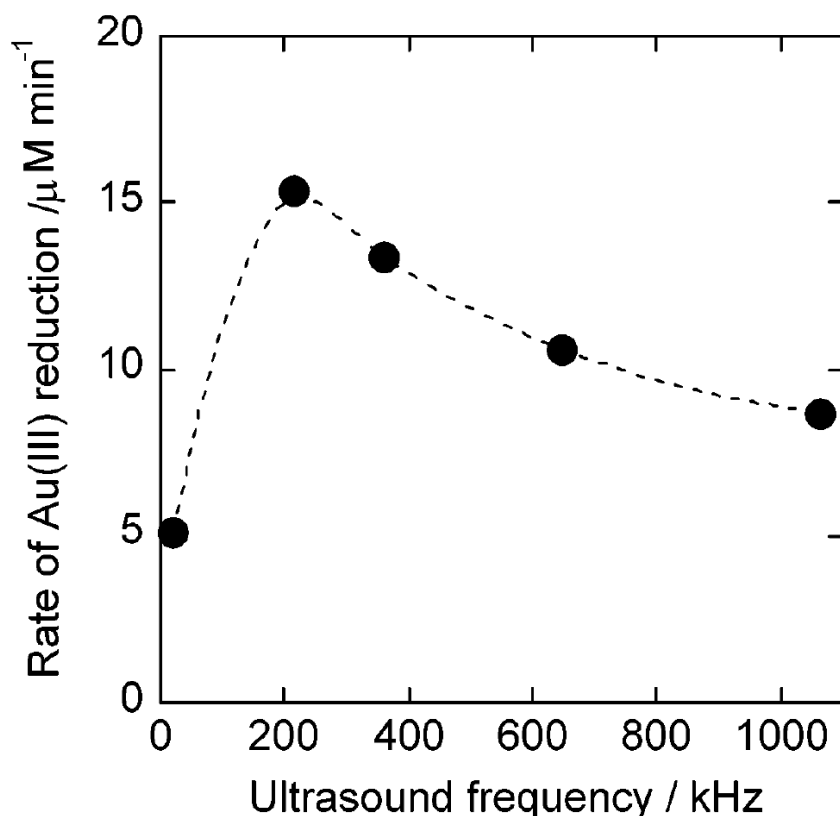
Figure 2. Rate of Au (III) reduction as a function of ultrasound frequency. Au (III): 0.2 mM, 1-propanol: 20 mM, atmosphere: Ar, ultrasonic power: 0.1 W mL^{-1}. Reprinted with permission from Ref. (109)

Copyright © 2005 American Chemical Society.

These variations are explained by detailing the chemical reactions involved in forming these nanoparticles through the presence of organic additives, which had been previously reported(110–113).

(1)	$H_2O \rightarrow ^-OH + ^+H$
(2)	$RH + ^-OH\ (^+H) \rightarrow ^+R + H_2O\ (H_2)$
(3)	$RH \rightarrow$ pyrolysis radicals and unstable products
(4)	$Au(III) +$ reducing species $(^+H,\ ^+R,\ etc.) \rightarrow Au(0)$

*RH denotes an organic additive

The first three reactions show the formation of the reducing radicals and reductants by the ultrasound with (1) sonolysis of water, producing ^+H (a primary sonochemistry reaction detailed previously), (2) Formation of ^+R and H_2 through the reaction of RH with ^-OH or ^+H, (3) Formation of pyrolysis radicals and hazardous products through the pyrolysis of RH and H_2O, and (4) the reduction of Au(III) into Au(0) by reacting with the various reducing species in a series of complex secondary steps[112].

From the fourth reaction, it can be inferred that the amount of reducing radicals produced in the initial reactions directly correlates with the reduction rate, and the amount of primary and secondary radicals produced depends on the efficiency of the cavitation at different frequencies. Different frequencies can influence several of the following factors[109]:

(1) Temperature and pressure inside the cavitation bubbles.
(2) Distribution and number of bubbles
(3) Size and duration of bubbles
(4) Shape, dynamics, and symmetry of the bubble collapse
(5) Various effects on other elements that might be present in the reaction, such as organic solvents (in the case of the Au(III) reduction, 1-propanol), secondary radicals, etc. which directly influence the temperature of the reaction.

While these factors are widely understood, the extent to which each factor influences radicals' resulting production is tough to quantify. This is because all these factors are heavily correlated, and it is not feasible to alter one without affecting the others to obtain different results for each one. What can be quantified is the overall effect that different ultrasound frequencies have on

reaction rates depending on agents used to alter reactions. As we saw previously in [Figure 5], the 213 kHz frequency corresponds to the highest reduction rate of Au(III) in the presence of 1-propanol, with the size distribution of the resulting gold nanoparticles and a TEM scan showing the structure of the nanoparticles at this frequency can be seen in [Figure 3].
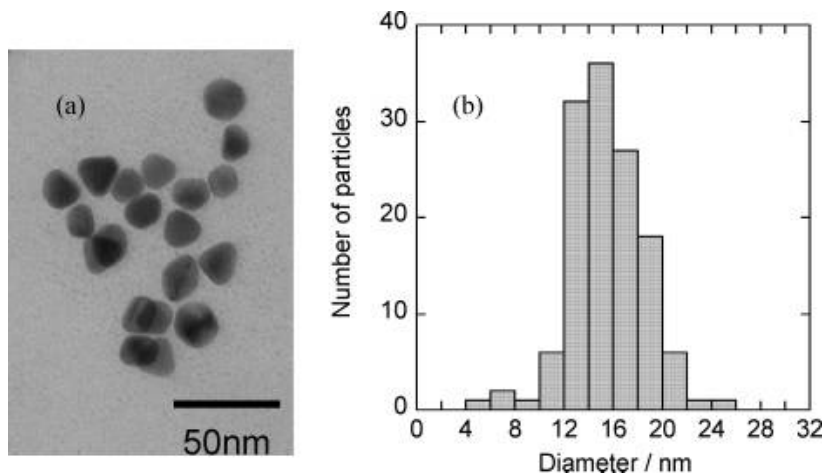
Figure 3. (a) TEM micrograph of Au nanoparticles synthesized after 120 min irradiation of 213 kHz ultrasound. (b) Histogram for the size distribution of Au nanoparticles. Reprinted with permission from Ref. (109)

Copyright © 2005 American Chemical Society.

Another study tested the various factors detailed previously for water sonolysis without any other element present(114) and found that the most activity was found within the 205 kHz to 629 kHz range. Through these alterations, individual events can be qualitatively depicted [Figure 4], showing how increases in frequency affect them. Their main conclusion from these variations was that at lower ultrasonic frequencies, a significant fraction of cavitation bubbles will collapse asymmetrically and that at higher ultrasonic frequencies, more excellent gas and volatile species flux will occur.
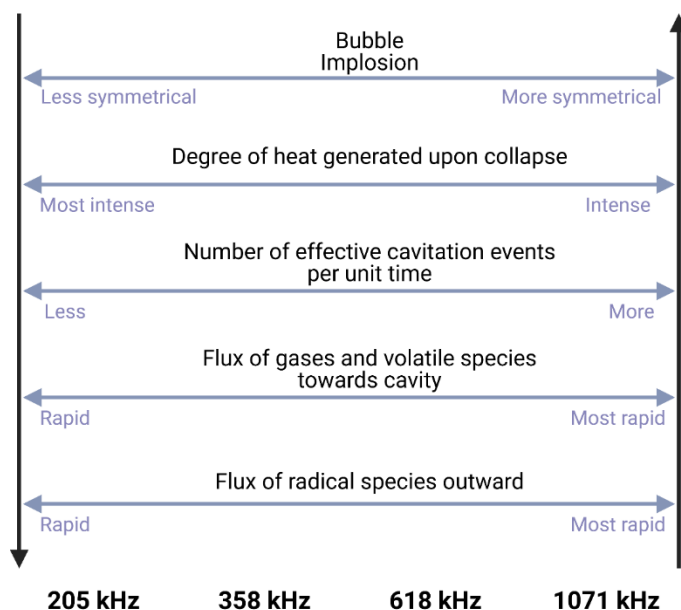
Figure 4. Summary of different acoustic cavitation events as a function of frequency through continuous irradiation and gas sparging. The vertical arrows indicate hierarchical importance regarding sonochemical activity as a function of frequency. Created with BioRender.com

Sonochemical synthesis can also be used to produce nonspherical nanoparticles such as nanorods(115), nanobelts(116), nanodecahedra(117), nanoplates(118). The referenced examples provide each nanoparticle type with gold as their main element, but ultrasound has been used to synthesize nanoparticles from a wide range of noble metals. Some noteworthy examples include, as mentioned previously, the use of ultrasound to synthesize core-shell nanoparticles. $PtCu_3$(119), PdAg(120), and Palladium with other first-row transition metal particles such as Ni, Co, Fe, Mn(121).

Silver nanoclusters of minimal size (<2nm) and remarkably high fluorescence can also be made using ultrasound by employing poly(methacrylic acid) as a capping agent(122). This is needed to make silver nanoparticles of this size since Ag nanoclusters tend to grow continuously in aqueous solutions. The capping agent not only stabilizes the nanoparticles but also protects them after cavitation. Previously this capping agent was used to synthesize silver nanoclusters with other methods such as radiolytic, chemical, and photochemical reductions of silver salts(123–126). The combination of the sonochemical method in conjunction with the capping agent demonstrates the potential of these types of synthesis methods, as they often provide more straightforward and inexpensive alternatives to traditional methods (and in this case, a more effective method, as clusters of this size were not previously possible and were not able to exhibit fluorescence).

25

Aside from noble metals, oxides and hydroxides can also be produced and shaped to form various nanoparticles. Nanoparticles from metal oxides are formed through sonochemistry by interacting radicals resulting from cavitation, and subsequent oxidation occurs. Sonohydrolysis can also be used as a method to induce oxidation and formation of nanostructures. One essential oxide often synthesized through sonochemistry is zinc oxide (ZnO). Some properties that make this material of high interest are its antimicrobial properties, photocatalytic properties, and its ability to serve as a wide bandgap semiconductor. For the fabrication of a nanostructured ZnO layer to be used as an electrochemical sensor matrix, two different types of nanoparticles (1D nanorods and 2D nanoflakes) from this material are synthesized, and both are produced through sonochemistry in a single step(127). This layer was grown on a Si substrate by applying ultrasound irradiation to a Zn salt mixed with hexamethylenetetramine to act as a shaping agent. ZnO nanostructures of this nature exhibit higher chemical stability, high catalytic activity, and biocompatibility than bulk materials for this nature's electrochemical sensors.

In a similar process, ZnO's antimicrobial properties have been used in another one-step sonochemical process where the nanoparticles were synthesized and assembled on a textile surface to produce an antimicrobial surface(128). This textile and paper coating process through sonochemical synthesis is also possible with other metallic compounds such as silver(129) and copper oxide(130). The mechanisms by which these nanolayers prevent and inhibit the growth of microbes are not well understood, but they have been verified to be effective against E. coli and S. aureous, sensitive to the precursors of the nanolayers. These compounds' vast versatility to be used as antimicrobial coating while maintaining high biocompatibility levels with meager production costs (mainly due to the simplicity of the sonochemical procedures involved) pose for a promising new wave of nanomaterials and coatings for industrial applications. These modifications that these coatings introduce to surfaces can also alter the surfaces' hydrophilicity, opening an even greater field of potential applications(92).

Physical effects of ultrasound

High-intensity ultrasound also has various physical effects that can alter in various ways the formation of nanomaterials, with these effects mainly being:

- Microjet formation

- Turbulence
- Microstreaming
- Shock wave formation
- Interparticle collisions in slurries

All of which can have different degrees of impact on the synthesis processes. All these effects result from the same phenomenon that causes sonochemical processes to occur: the cavitation resulting from the collapse of the bubbles introduced by the ultrasound waves. When the collapse occurs in the liquid medium employed for the process, shockwaves are generated and then propagated throughout the medium. The shapes of the bubbles –which were also described in the previous section– are crucial for forming microjets. If a bubble is formed near a solid, then that bubble will be non-spherical, and when it collapses, the deformations will cause a significant disproportion in the ejection of the surrounding liquid. These displacements are known as a microjet, and the immense pressures inside the bubble cavitation make them a significant factor to consider as they can impact surfaces and eject materials. The vibrations and cavitation events induced by high-intensity ultrasound cause rapid streams and currents in the medium as well as intense mixing, all factors that contribute to ultrasound being an effective method for liquid mixing, eroding surfaces of solid bulk materials, and induce particle collisions in emulsions and solid-liquid mixtures(131–133).

One good example of a process involving the use of the physical properties of ultrasound is the production of ZnO hierarchically structure microspheres(134). Hierarchical structures refer to the types of nanostructures composed of substructures such as nanoparticles, nanorods, nanoplates, nanoflakes, etc.

The study referenced states that this material's hierarchical structures (ZnO) were developed because of the need to improve photovoltaic performances of dye-sensitized solar cells(135,136). Previous candidates for this user, such as crystalline aggregates of titanium dioxide (TiO_2) and crystalline ZnO, were effective in these applications, but the interparticle boundaries within the produced structures were big enough to hinder the transport of photogenerated electrons(137,138). For this reason, hierarchical structures with the capability for the free movement of electrons within its structure were necessary. The components of the hierarchical structure itself are also other variables that can affect its characteristics. A

nanosheet-based hierarchical structure showed better capabilities for electron transport than nanocrystal aggregates(139,140).

Many methods were previously used to produce nanosheet-based hierarchical structures, including chemical bath deposition(141), hydrothermal approaches(142), annealing(143), electrodeposition(144), and direct precipitation(145). Direct precipitation being the simplest of this group since it is a one-step process. The main disadvantages of direct deposition are the lack of uniformity and difficulty in controlling the hierarchical structures' structure. The ultrasound process developed from ultrasonic irradiation into the previously established natural precipitation process(146). The authors' main improvements brought by the introduction of ultrasound are an acceleration of nucleation and better diffusion in the medium, both physical effects of ultrasound. These effects resulted in higher accuracy in shaping structures of the nanolayers, nanoparticles, and their assembly into hierarchical structures. These improvements also allowed for the hierarchical structures to be assembled in 15 minutes and without templates that were needed in the previous processes of direct precipitation without the integration of ultrasound. A comparison between the resulting nanoparticles from both processes can be seen in [Figure 5].
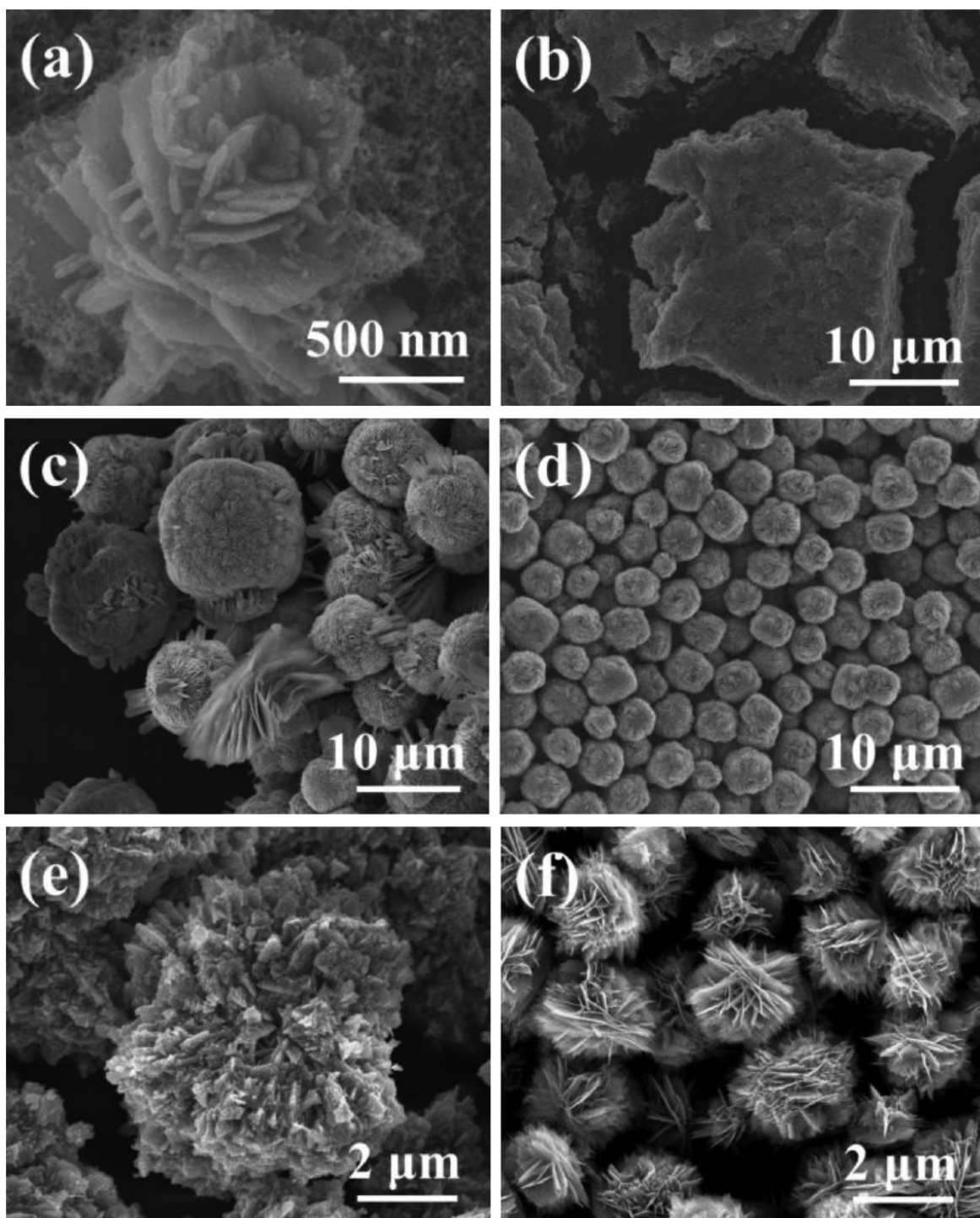
Figure 5. SEM images of ZnO samples were obtained at different conditions. (a) and (b). In-situ observation of sample A at t = 15 min; (c) sample A; (d) sample B; (e) sample C; (f) sample D. Reprinted with permission from (134).

Copyright © 2013 American Chemical Society.

In this figure, we can see four different samples in different conditions, with samples A and B having the same concentration of their precursors (0.5 M of OH⁻ and 0.1M of Zn^{2+}), with the difference being that for A, ultrasound was not used, and for B ultrasound was utilized. Samples C and D had different precursors concentrations than the first two samples, with double the

number of Zn^{2+} (0.5 M of OH^- and 0.2M of Zn^{2+}), and ultrasound was used for D but not for C. The figure shows all four samples at t = 15min. With the different samples established, in [Figure 8], we have (a) and (b), which show Sample A at different magnifications and unfinished structures can be seen, indicating a slow synthesis process with just direct precipitation. The acoustic cavitation event generates an actual amount of energy transferred mainly to the nucleation process, causing a significant acceleration to this segment of the hierarchical structures' formation. Sample A needed 40 minutes to complete its formation of hierarchical structures without the use of ultrasound, and the resulting nanoparticles were comparatively nonuniform with large size variations (from 3 to 13μm). Sample A at t = 40 min is shown in [Figure 8(c)]. Sample B, as mentioned previously, employed ultrasound and can be seen in (d) at the same amplification of (c). It is visibly a much more homogeneous group of hierarchical structures than sample A. The sizes from sample B range from 2 to 5μm. The authors attribute this impressive uniformity to the strong blast and high-speed microjet produced by the acoustic cavitation, which resulted in effective nanocrystal dispersal and ionic diffusion. One crucial factor for forming specific ZnO-based nanostructures in this medium is the amount of excess. OH^-, which determines the resulting architecture drastically. As mentioned previously, samples C and D had double the amount of Zn^{2+} concentration and less OH^- excess. Sample C can be seen in [Figure 8(e)] where each nanoparticle's hierarchical structure was around 6μm and featured a different hierarchical structure than the other samples, which were not suitable for the intended use. Despite having the same precursor concentrations as sample C, Sample D featured hierarchical structures of 2μm and the desired 2D nanosheet-based hierarchical structures. Since sample C was prepared through direct precipitation and sample D through ultrasound-assisted direct precipitation, these two samples demonstrate the importance and benefits of ultrasound in nanoparticle synthesis. Sample D also demonstrated that fast and homogeneous nucleation coupled with an organized, non-aleatory aggregation could compensate for lack of excess OH^- in obtaining a determined architecture for a hierarchical structure (in this case, a nanosheet-based structure).

Ultrasonic spray pyrolysis for nanomaterials

The physical effects of ultrasound are used in another method called ultrasonic nebulization (also sometimes referred to as ultrasonic atomization). Ultrasound radiation of liquid mediums causes the ejection of liquid droplets on the medium's surface, and these droplets

are the primary manifestation of ultrasonic nebulization. The average size of the droplets produced by ultrasonic nebulization can be calculated using Lang's equation:
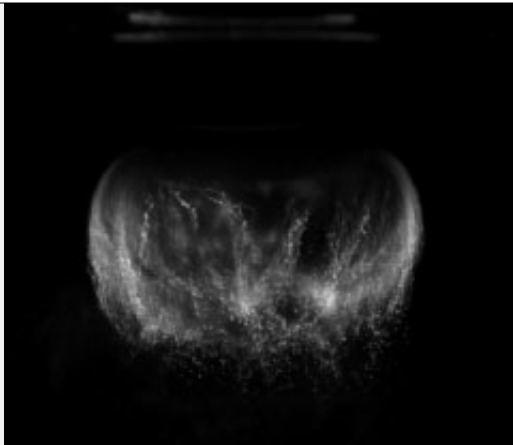
$$D = 0.34 \left(\frac{8\pi\gamma}{\rho f^2} \right)^{1/3}$$

In this equation D represents the droplet's diameter, γ the liquid's surface tension, ρ the liquid density, and f the ultrasonic irradiation frequency[147].

For syntheses involving ultrasonic nebulization, we can consider each droplet as a minuscule chemical reactor that can be used to produce chemical reactions by introducing light, heat, or other stimuli. Ultrasonic nebulization can be used to generate a dense mix regardless of the gas's flow rate. It can be scaled with relative ease for a variety of applications, including plant production. The properties (temperature, frequency, etc.) and precursors (templates, solvents, additives, etc.) of these processes can be modulated to achieve different nanostructures.

Ultrasonic spray pyrolysis is not directly involved in chemical reactions, the role of the ultrasound in this process is to provide phase isolation of one microdroplet reactor to another[148]. This is in contrast with sonochemical approaches, which are mainly thermally driven. Another important distinction is that for sonochemistry the ultrasound employed is of high intensity and with a low frequency of around 20kHz, and for ultrasonic spray pyrolysis, the intensity is a low and high frequency of around 2MHz.

Some of the other significant differences between sonochemical approaches and ultrasonic spray pyrolysis are highlighted in [Table 1].

	SONOCHEMISTRY	ULTRASONIC SPRAY PYROLYSIS
REACTION SITE	Gas bubbles	Liquid microdroplets

CONDITIONS	~5000 K, 1000 bar	500–1300 K, 1 bar
REACTANTS	Volatiles primarily	Nonvolatile solutes
COOLING RATES	$>10^{10} K\ s^{-1}$	$10^4 K\ s^{-1}$
TEMPLATING	Easy	Easy, easy nanocomposites
HEATING ZONE	Single extreme hot zone	Multiple hot zones possible
SCALABILITY	Scalable: kg/day	Easily scalable: ton/day
PARTICLE SIZE CONTROL	Nano- and submicron-sized particels	Typically submicron-size, but nanoparticles possible
COMPOSITION CONTROL	Easy	Easy
ANISOTROPIC SHAPES	Yes	No
HOLLOW STRUCTURES	Yes	Yes
CORE/SHELL STRUCTURES	Yes	Yes

Table 1. Comparison of the characteristics between sonochemistry and ultrasonic spray pyrolysis. Images reprinted with permission from Ref. (148)

Ultrasonic spray pyrolysis as a synthesis tool provides several advantages over alternative and traditional approaches. It can produce submicron-sized spherical particles with minimal impurities, a high degree of control of the nanoparticle composition, and ease of operation over extended periods(149,150). Compared to solid-phase or liquid-phase techniques such as direct precipitation and hydrothermal methods, which require batch reactions to produce materials, ultrasonic spray pyrolysis is a continuous flow process that allows for small and large scale productions of materials with low variability(148). This characteristic also offers a unique advantage in that ultrasonic spray pyrolysis can prepare many multi-component materials that would be significantly harder with other methods, especially considering the high degree of control it offers over the physical and chemical compositions of compounds.

An ultrasonic spray pyrolysis apparatus can be seen in [Figure 6] and consists of the ultrasound transducer placed in the bottom of the container that houses the precursors. The container is equipped with a gas stream dedicated to carrying the steam generated into a tubular furnace, where a collector traps the mist produced by the ultrasound. Deposition occurs in the furnace, where the substrates (such as silicon or glass) are placed. As explained by Suslick et al.(148), additional furnaces can be attached at the end of the single surface to increase the droplets' residence time in heated areas or introduce multiple temperatures. They also state that the

authors' research group's apparatus to perform ultrasonic spray pyrolysis is based on an inexpensive, high-frequency ultrasound generator obtained from a household humidifier, highlighting the low cost and great accessibility that this synthesis approach offers.
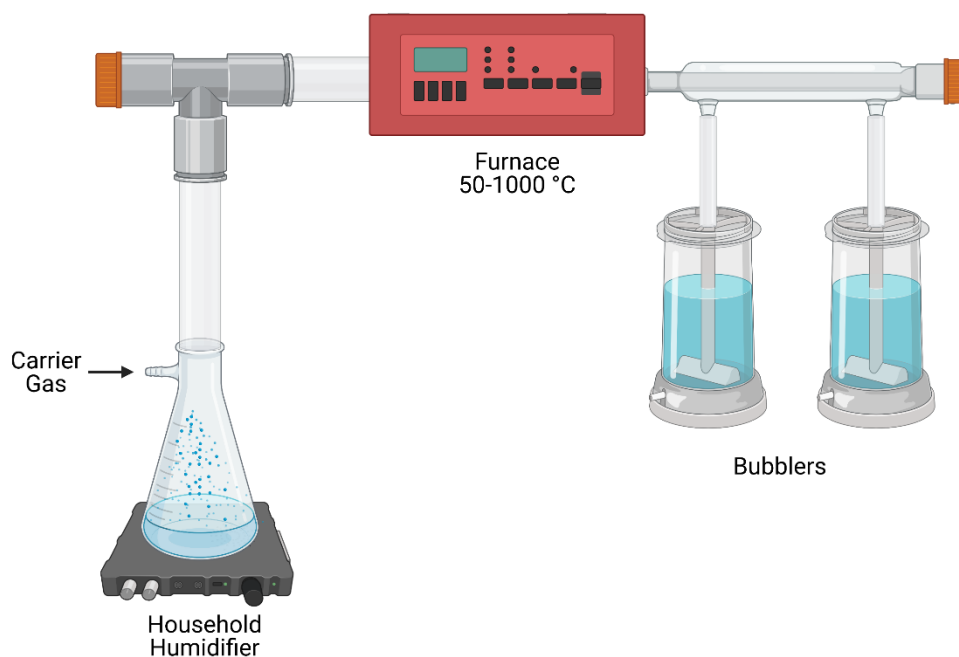

Figure 6. Basic schematic illustration of a standard ultrasound spray pyrolysis apparatus.

Created with BioRender.com

The synthetic process of ultrasonic spray pyrolysis involves droplet generation, solvent evaporation, solute diffusion, precipitation, decomposition, and densification. A simplified graphical depiction of this process can be seen in [Figure 7].
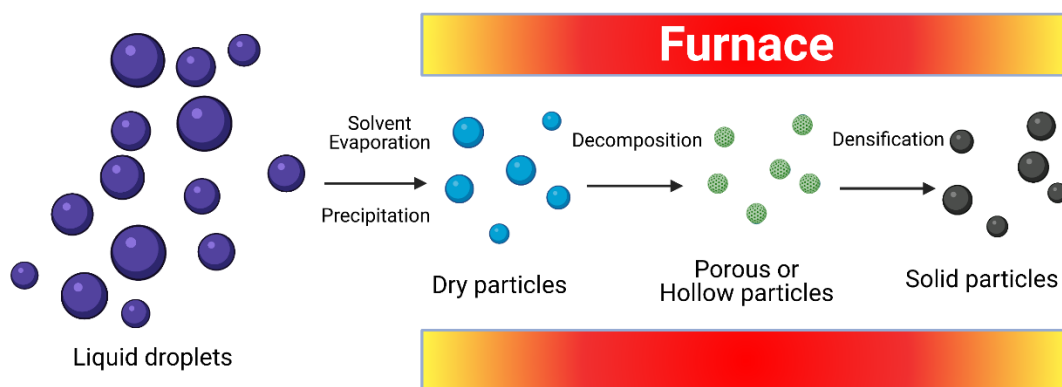
Figure 7. Simplified ultrasound spray pyrolysis process.

Created with BioRender.com

Sonocrystallization and sonofragmentation

The first reported use of ultrasounds to produce crystalline materials dates to the year 1927(151). These early reports indicated marginal effects of ultrasonic irradiation on supersaturated solutions and supercooled melts. These early findings caused the development of these ultrasound applications to remain unexplored until the 1950s when many of the documented benefits of ultrasounds in crystallization were first reported. These reports include research from the Soviet Union that highlighted the reduction of grain size when ultrasound irradiation was integrated into the crystallization process, among other variations of the crystallization kinetics found with ultrasounds' introduction (152). In the 1960s, ultrasound-based approaches gained notoriety as several studies found them to induce the formation of micro-sized uniform particles with pharmaceutical agents(153–155), and many mechanisms for sonocrystallization were also proposed during this era(156).

Nowadays, ultrasound effects are understood to originate mainly from the ability of ultrasounds to induce crystal nucleation. Crystal nucleation is a complex and widely studied field, with its variations being mainly measured by analyzing the metastable zone width and induction time. Many studies have analyzed and compared their induction time in organic molecules with similar findings and conclusions(157–159). Among these findings, Guo et al.(158) measured the induction time for the antisolvent crystallization of roxithromycin. To measure crystallization and nucleation times, water was introduced into an acetone-based roxithromycin solution and monitored using laser light scattering. This experiment was done with and without the presence of ultrasound to be able to measure the impact ultrasound has on the crystallization process with different supersaturation degrees. In the tests that integrated ultrasound irradiation,

the induction time for roxithromycin decreased consistently and dramatically at all the various supersaturation degrees (158). The authors attribute these reduced induction times to an acceleration in diffusion in the presence of ultrasound.

Ultrasound's physical properties applied to crystallization techniques help inducing nucleation, but it is also an essential tool to fragmentation crystals in an ultrasonic field. In contrast to a metal powder sonication which consists of malleable elements and agglomerates when exposed to ultrasonic irradiation (mainly due to collisions caused by gravitational shockwaves, ionic crystals sonicated as slurries result in fragmentation of the crystals(160). In experiments carried out using aspirin crystals suspended in decane which were then irradiated with ultrasounds, particle size averages did not fluctuate with the initial particle concentration as would be expected if interparticle collisions drove the sonofragmentation. The authors suggest that shock wave-particle interactions mainly drive sonofragmentation.

The acoustic cavitation and its extreme local temperatures and pressures generated by high-intensity ultrasound makes it a potent and versatile tool to produce nanomaterials. Another important aspect of the properties of ultrasound is the ability to selectively use the acoustic cavitation's chemical and physical effects in an extensively large number of ways and combinations. This ultimately allows for the synthesis of a wide range of nanostructured materials that would not otherwise be possible to produce. For these reasons, its low cost, and accessibility, ultrasound-mediated synthesis methods remain as invaluable tools for the synthesis of nanomaterials.

Chapter V

Ultrasounds for Quantum Dot synthesis: diversity, features, bioapplications, comparisons, strengths, and weaknesses

As seen in the previous sections, Quantum Dots encompass a wide range of materials with different functions and combinations of said materials. The effectiveness of these QDs for their intended uses is heavily dependent on several factors, including size dispersion, surface uniformity, yield, among others. The methods used to achieve the specific characteristics with precision vary with the different compositions, precursors, architecture, and sizes. In this context, ultrasound can be applied in various ways to synthesize or enhance previously existing QD synthesis methods. The physical and chemical properties of ultrasound irradiation can be selectively applied to a medium according to the precursors and the desired outcome. In this section, the performance of ultrasound-mediated synthesis methods will be evaluated and compared to other methods used for a given QD type or element. This section's main objective is to highlight the advantages, unique features, and weaknesses and establish the current relevance in the QD synthesis field. Due to the vast number of QDs that can be synthesized through ultrasound-related approaches, two QD types with abundant methods and literature were chosen to contrast ultrasound methods with the highest number of approaches possible.

Molybdenum Disulfide QDs

MoS_2 QDs, classified as transition metal dichalcogenide QDs, have been synthesized through various strategies(161), including the hydrothermal method(162), a bottom-up approach. Among the top-down approaches, MoS_2 QDs have been produced using an ultrasound-mediated mechanical exfoliation(163), chemical exfoliation(164), electrochemical method(165,166), emulsion method(167), solvothermal method(168), thermal ablation(169), and combined methods(170,171).

The ultrasound-mediated synthesis of MoS_2 QDs involves using ultrasound irradiation to exfoliate the bulk MoS_2 into monolayers which can then be processed into QDs. The first step in this process involves processing natural mineral molybdenite with high-intensity ultrasonic

irradiation in a pressured batch reactor, producing MoS_2 nanosheets. MoS_2 QDs can be then produced by immersing the MoS_2 nanosheets into ethylene glycol at atmospheric pressure for 24 hours. This method can produce QDs from other layered materials, such as WS_2, $TaSe_2$, $MoTe_2$, $MoSe_2$, $NbSe_2$, $NiTe_2$, BN, Bi_2Te_3(172–174).

A similar method employing ultrasound-mediated exfoliation of MoS_2 nanolayers was developed by Dai et al.(163), which added sulfuric acid to the medium. Ultrasonic irradiation caused the sulfuric acid molecules to permeate between the bulk MoS_2 layers, all this resulting in MoS_2 QDs with superior blue emission excitation-independent behavior. The full steps for the sulfuric acid-mediated process can be seen illustrated in [Figure 8].
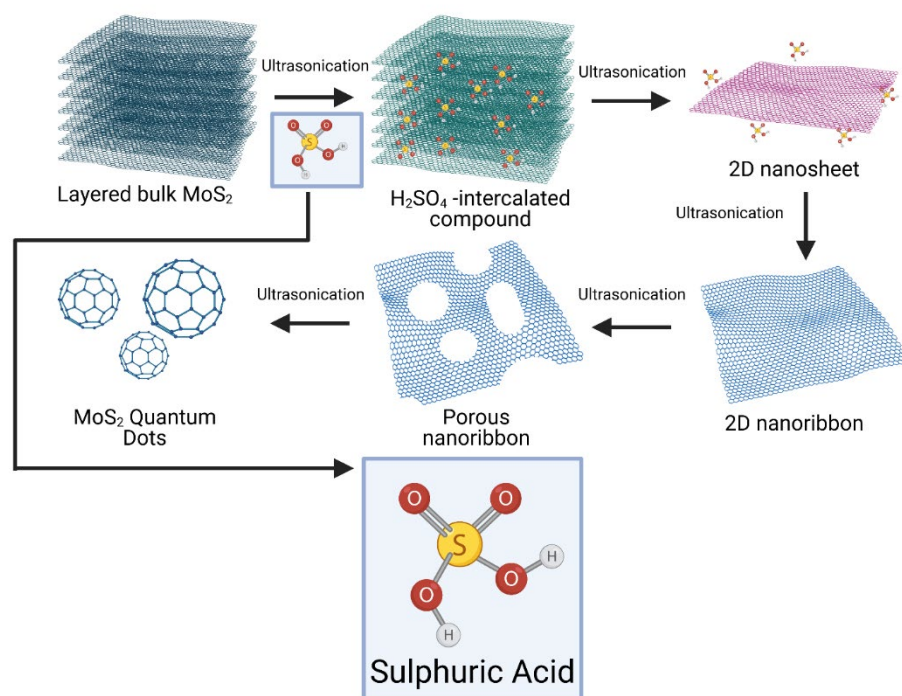
Figure 8. Schematic representation of a proposed mechanism for preparing MoS₂ QDs.

Created with BioRender.com

Combined methods in the studies included in this section employ ultrasonic irradiation to modify or enhance other methods. One of these methods involves using ethanol-thermal treatment of MoS_2 powder while ultrasound irradiation is emitted(171). This method allowed for the successful breakdown of bulk MoS_2 into MoS_2 QDs, with the resulting QDs being of small size (with a lateral size distribution from 1.2 to 4.2 nm, the average size being 2.9 nm), highly stable, and possessing two-photon fluorescence, which was suitable for cell imaging.

Another ultrasound-related combined method involved an ionic intercalation method combined with sonication. This combined method was performed in an N-methyl pyrrolidone (NMP) medium where MoS_2 powder was subjected to ultrasonic irradiation, which resulted in the formation of MoS_2 nanosheets as well as a comparatively small amount of MoS_2 QDs. When alkali metal ions were added to the process during the sonication step, the exfoliation efficiency was improved, yielding more QDs(175). A unique property from these QDs was their variable fluorescent emission with varying excitation wavelengths, making them excellent candidates for potential uses in cell imaging and the optoelectrical field. One downside the study reported was the low quantum yield but noted that the quantum yield increased from 0.99% to 4.84% through sodium hydroxide in the post-synthesis period.

Wet ground was also employed coupled with ultrasound irradiation in another study. This method consisted of wet grinding bulk MoS2 in an NMP medium, which was then subjected to probe sonication in a different medium, comprised of NMP and 1,2-dichlorobenzene. The resulting QDs had lateral size distributions of 2 to 5 nm and blue emission when excited(170).

Despite the many methods available for MoS_2 QD synthesis, synthetic synthesis methods still need to be further developed. Most of the current synthetic approaches result in low quantum yields and blue emission (including ultrasound-based mechanical approaches), resulting in negative biological applications. On [Table 2], we can observe that despite low quantum yields for most methods, the mechanical exfoliation-sulfuric acid assisted ultrasonic method (163) provided a relatively high quantum yield compared to other methods, and the addition of ultrasound in combined methods produced QDs with better quantum yields and even allowed for variable emissions. Sonication is present in many more methods during the early stages to produce nanosheets from bulk MoS_2 materials since nanosheets are the most effective

and consistent precursor to form MoS_2 QDs.

Carbon Quantum Dots or Carbon Dots (CQDs/CDs)

As stated previously, the term "carbon dots" is commonly used to refer to a general group of carbon-based QDs that consist of graphene QDs, polymer QDs, carbon QDs, and carbon dots. CQDs possess some properties and advantages that make them stand out among other QDs, their meager production cost and simplicity, often putting them as the first choice for QD researchers(186). Some of their other notable properties are their ultra-small particle sizes, excellent biocompatibility, and outstanding optical properties.

METHOD	PRECURSORS	QY	EMISSION	REFERENCE
CHEMICAL EXFOLIATION (NA INTERCALATION)	Bulk MoS_2 powder	11%	430 nm	(164)
CHEMICAL EXFOLIATION (LI 2H-MOS2 POWDER - 420 NM INTERCALATION)	$2H-MoS_2$	-	420 nm	(176)
MECHANICAL EXFOLIATION-ULTRASOUND METHOD	Natural molybdenite	-	∼480 nm	(174)
MECHANICAL EXFOLIATION-SULFURIC ACID ASSISTED ULTRASONIC METHOD	MoS_2 powder	9.65%	414 nm	(163)
ELECTROCHEMICAL METHOD	Bulk MoS_2 powder	-	∼400 nm	(166)
ELECTROCHEMICAL METHOD	MoS_2 nanosheets		401 nm	(165)
EMULSION METHOD	MoS_2 powder	-	∼ 480-540 nm	(167)
SOLVOTHERMAL METHOD	MoS_2 powder	-	461 nm	(168)
SOLVOTHERMAL METHOD	MoS_2 powder	-	463 nm	(177)
THERMAL ABLATION METHOD	Single layer MoS_2	-	548 nm	(169)
COMBINED METHOD (ULTRASONICATION+ ETHANOL-THERMAL METHOD)	MoS_2 powder	3.10%	428 nm	(171)
COMBINED METHOD (SONICATION+ION INTERCALATION)	MoS_2 powder	4.84%	∼500 nm	(175)
COMBINED METHOD (GRINDING+CO-SOLVENT SONICATION)	(Wet MoS_2 powder)	-	448 nm	(170)
HYDROTHERMAL METHOD	Sodium molybdate+L-cysteine	2.60%	402 nm	(162)
HYDROTHERMAL METHOD	Sodium molybdate+glutathione	∼10.3%	425 nm	(178)
HYDROTHERMAL METHOD	Sodium molybdate+dibenzyldisulfides	-	280 nm	(179)
HYDROTHERMAL METHOD	Sodium molybdate+thiourea	0.28%	406 nm	(180)
HYDROTHERMAL METHOD	Molybdenyl acetylacetonate+thioglycolic acid+Na_2S	-	420 nm	(181)
HYDROTHERMAL METHOD	Sodium molybdate+Na_2S+1,4-Diaminobutane	-	423 nm	(182)
HYDROTHERMAL METHOD	Ammonium molybdate+N-acetyl-L-cysteine+thiourea	-2%	480 nm	(183)
HYDROTHERMAL METHOD	$(NH_4)_2MoS_4+N_2H_4$	-	400 nm	(184)
HYDROTHERMAL METHOD	$(NH_4)_2MoS_4$+oleylamine	4.40%	575 nm	(185)

Table 2. List of different synthetic methods for MoS2 QDs. The methods involving ultrasound irradiation have been highlighted.

There are many methods with which CQDs can be produced, both bottom-up and top-down. Bottom-up approaches for CQD synthesis include the sonochemical approach, pyrolytic

method, template-mediated synthesis, microwave-induced synthesis, chemical processes, and reverse micelle method. Top-down approaches include laser ablation, electrochemical process, arc discharge, and plasma-assisted synthesis.

Sonochemistry (previously described as applying the chemical capabilities of ultrasound) is an invaluable tool in elaborating many carbon-based materials and industrial manufacturing processes in general(91). CQD synthesis's standard process through sonochemistry involves carbon precursors with a determined concentration in specific solvents and then subjected to ultrasonic irradiation. One example of these methods is preparing CQDs using acid- or alkali-assisted ultrasound treatment of glucose followed by CQDs' formation by ultrasound irradiation(187). Another example that results in nitrogen-doped CQDs involves sonochemically induced pyrolysis of carbon precursors inside the collapsing bubbles formed by the cavitation, producing highly photoluminescent nanoparticles(188). The main downside of these two examples is the involvement of catalysts, multi-step processes, which produce low yields and inconsistent results. More recent ultrasound-based methods have produced QDs with the sonication of a single material, eliminating the need for catalysts while also reducing the steps needed to a single one(189). This method involves placing 12mL of polyethylene glycol in a test tube and then immersed in a water/silicon oil where an ultrasonic probe is inserted around 1cm above the bottom of the tube where it releases emits irradiation. This sonochemical procedure can be illustrated with additional details in [Figure 9].
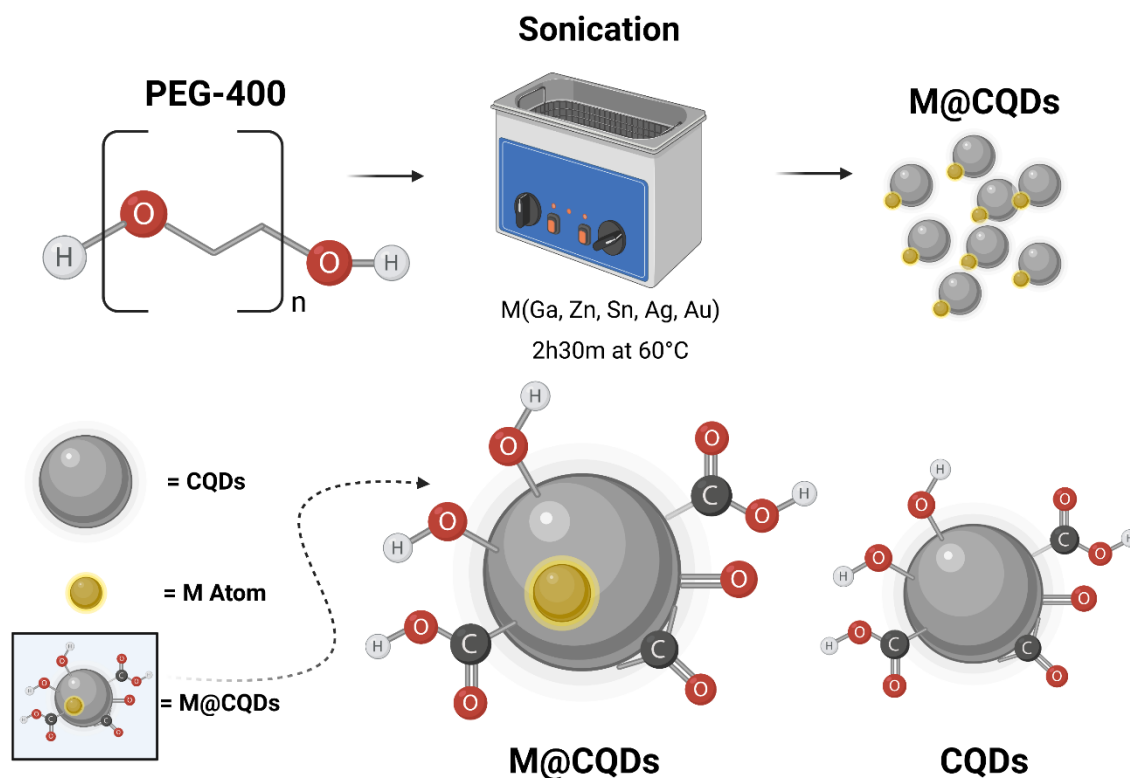
Figure 9. Synthesis procedure for CQDs and metal doped CQDs.

Created with BioRender.com

While CQDs have many potential synthesis routes, the synthesis of metal-doped CQDs can only be done through sonochemistry. The metals used for this process are low melting points, such as Ga, In, Bi, Sn, Pb, Cd, Sb, and Zn. In [Table 3], we can see a summary of the employed literature, and we can see that earlier method for CQD synthesis provided above-average quantum yields but not high enough to be very practical, considering they required the use of catalysts and produced low CQD yields.

METHOD	PRECURSOR	QY%	EMISSION COLOR	REF
ARC DISCHARGE	Carbon soot	1.6	Blue, yellow	(190)
ARC DISCHARGE	Oxidized carbon nanotubes	-	Blue to yellowish green	(191)
LASER ABLATION	Graphite	4-10	450-650 nm	(31)
COMBUSTION	Candle soot	0.8-1.9	Full color	(192)
ELECTROOXIDATION	Graphite	1.2	Blue, yellow	(193)
ELECTROCHEMICAL APPROACH	Graphite	8.9	450 nm	(194)
THERMAL OXIDATION	Citric acid, H2N(CH2)10 COONa	3	Visible to near IR	(195)
THERMAL PYROLYSIS	CA, ODE, HAD	53	Full color	(196)

41

	CA, EA	50	Full color	(197)
	CA, DETA	88.6	Blue to yellow	(198)
SUPPORTED SYNTHESIS	F127, Resol	11-15	Violet to yellow	(199)
SUPPORTD SYNTHETIC METHOD	F127, Resol	14.7	430-580 nm	(199)
MICROWAVE PYROLYSIS	Sacharide, PEG,	3.1-6.3	Blue to green	(200)
	Glucose, aminor acids	30-69	Blue, green, yellow	(201)
MICROWAVE ASSISTED	Folic acid	18.9	460 nm	(202)
SONOCHEMICAL	Glucose	7	Full color	(187)
SONOCHEMICAL	Glucose	7	Visible to near IR	(187)
HYDROTHERMAL SYNTHESIS	CA, EDA	80.6	Full color	(203)
	CA, L-cysteine	73	Deep blue	(204)
	Sodium citrate, Ammonium	68	Blue	(205)
	bicarbonate (NH_4HCO_3) CA, EDA	94	Blue	(206)
CHEMICAL METHOD	Carbohydrate	6-30	Full color	(207)
CHEMICAL OXIDATION	Acetic acid	-	Green	(208)
PLASMA TREATMENT	Benzene	-	Green	(209)
PYROLYTIC PROCESS	Citric acid and glutathione	80.3	Blue	(210)
TEMPLATE ASSISTED SYNTHESIS	Glycol	32	450-480 nm	(211)
REVERSE MICELLE	Glucose	35	435-550 nm	(212)
SONOCHEMISTRY	Polyethylene glycol (PEG-400)	~16	360 nm	(189)

Table 3. Literature summary of CQD synthesis methods through different techniques. CA: citric acid, PEG: polyethylene glycol, ODE: octadecene, HDA: 1-hexadecyl amine, EA: ethanolamine, DETA: diethylenetriamine, EDA: ethylenediamine, QY: quantum yield. Ultrasound-based techniques are highlighted.

Recent single-step methods allow for much more accessible procedures, with metallic doping becoming a unique method that opens many practical possibilities for CQDs in bioimaging, cell labeling, drug delivery, catalysts, polymerization, ointment, antibacterial, dye degradation, supercapacitors, and superconducting devices.

Chapter VI

Conclusions

This review discussed and summarized several factors surrounding the characteristics, applications, and interactions of Quantum Dots and Ultrasounds. A key takeaway from this bibliographic research is the importance of ultrasounds in synthesizing Quantum Dots and nanoparticles, which is mainly due to the extreme conditions it can cause in a liquid medium. The other important aspect of ultrasound is its cost and accessibility; while there is high-cost industrial ultrasound machinery, many of the QDs we have overseen in this review can be synthesized with ultrasound irradiation from low-cost ultrasound plates found in commercial humidifiers (even if they do not have the best properties). Ultrasounds can also provide unique synthesis opportunities to produce unique QDs since the qualities of the cavitation bubbles can be adjusted using different intensities and wavelengths.

As for Quantum Dots, during the past decade, they have demonstrated most of their potential value hypothesized during previous decades. QDs have been successfully integrated into various fields and specific applications, especially in the biomedical field, with an increasing number of uses in oncology treatments, tissue engineering, regenerative medicine, imaging applications, and even drug delivery. This wide variety of possible applications is due to the different materials that have been synthesized into Quantum Dots. One limitation of Quantum Dots, mainly when applied to biomedical or biological applications, is their potential for toxicity enhanced by procedures involving hazardous chemicals for their synthesis. Toxicity can be caused either by accumulating QDs in sensitive areas or contamination of QDs with said chemicals. Some damage can also be caused by the emission of unwanted wavelengths from the QDs when irradiated, namely, the blue spectrum (450–485 nm), which can cause adverse biological effects. Ultrasound processes have proven to mitigate these problems in many cases by enhancing existing methods to produce more effective QDs with better quantum yields, narrower size dispersions, and a more precise emission spectrum.

In some cases, ultrasound irradiation has even eliminated the need to include dangerous reactive species when ultrasound has been used to induce all the necessary reactions to synthesize the QDs. Despite the massive advancements both ultrasound procedures and QD synthesis methods

have gained, there are still many challenges to improve their respective uses. Since acoustic cavitation is an almost instantaneous event with drastic changes in temperature and pressure, many chemical and physical interactions occur during these events, and most of the reactions involved in many of the currently used processes are still not fully understood, and further research in this area is encouraged. The complete understanding of the mechanisms involved in QD synthesis during cavitation could prove to be revolutionary to push QDs closer to their medical and industrial potential.

REFERENCES

1.   Ekimov A, Onushchehko A. Quantum Size Effect in Three-Dimensional Microscopic Semiconductor Crystals. ZhETF Pis Ma Redaktsiiu. 1981 Aug 31;34:363.

2.   Reed M, Randall J, Aggarwal R, Matyi R, Moore T, Wetsel A. Observation of discrete electronic states in a zero-dimensional semiconductor nanostructure. Phys Rev Lett. 1988 Feb;60(6):535–7.

3.   Michalet X. Quantum Dots for Live Cells, in Vivo Imaging, and Diagnostics. Science. 2005 Jan 28;307(5709):538–44.

4.   Ashoori RC. Electrons in artificial atoms. Nature. 1996 Feb;379(6564):413–9.

5.   Ziman JM. Principles of the Theory of Solids [Internet]. 2nd ed. Cambridge University Press; 1972 [cited 2021 Mar 25]. Available from: https://www.cambridge.org/core/product/identifier/9781139644075/type/book

6.   Zhang Y, Liu Y, Li C, Chen X, Wang Q. Controlled Synthesis of Ag2S Quantum Dots and Experimental Determination of the Exciton Bohr Radius [Internet]. American Chemical Society; 2014 [cited 2021 Mar 25]. Available from: https://pubs.acs.org/doi/pdf/10.1021/jp501266d

7.   Kargozar S, Hoseini SJ, Milan PB, Hooshmand S, Kim H, Mozafari M. Quantum Dots: A Review from Concept to Clinic. Biotechnol J. 2020 Dec;15(12):2000117.

8.   Klusoň P, Drobek M, Bártková H, Budil I. Welcome in the Nanoworld. Chem Listy [Internet]. 2007 May 15 [cited 2021 Mar 28];101(4). Available from: http://www.chemicke-listy.cz/ojs3/index.php/chemicke-listy/article/view/1796

9.   Eftekhari A. Nanostructured Materials in Electrochemistry. John Wiley & Sons; 2008. 491 p.

10.   Goswami N, Giri A, Kar S, Bootharaju MS, John R, Xavier PL, et al. Protein-Directed Synthesis of NIR-Emitting, Tunable HgS Quantum Dots and their Applications in Metal-Ion Sensing. Small. 2012;8(20):3175–84.

11.   Mirzai H, Nordin MN, Curry RJ, Bouillard J-S, Zayats AV, Green M. The room temperature phosphine-free synthesis of near-infrared emitting HgSe quantum dots. J Mater Chem C. 2014 Feb 27;2(12):2107–11.

12.   Tang X, Ackerman MM, Guyot-Sionnest P. Thermal Imaging with Plasmon Resonance Enhanced HgTe Colloidal Quantum Dot Photovoltaic Devices. ACS Nano. 2018 Jul 24;12(7):7362–70.

13.   Wang J, Wang X, Tang H, Gao Z, He S, Li J, et al. Ultrasensitive electrochemical detection of tumor cells based on multiple layer CdS quantum dots-functionalized polystyrene microspheres and graphene oxide – polyaniline composite. Biosens Bioelectron. 2018 Feb 15;100:1–7.

14.   Fan X-B, Yu S, Wang X, Li Z-J, Zhan F, Li J-X, et al. Susceptible Surface Sulfide Regulates Catalytic Activity of CdSe Quantum Dots for Hydrogen Photogeneration. Adv Mater. 2019;31(7):1804872.

15.   Park Y, Yoo R, Park S ryull, Lee JH, Jung H, Lee H-S, et al. Highly sensitive and selective isoprene sensing performance of ZnO quantum dots for a breath analyzer. Sens Actuators B Chem. 2019 Jul 1;290:258–66.

16.   Wang Y, Wang P, Wu Y, Di J. A cathodic "signal-on" photoelectrochemical sensor for Hg2+ detection based on ion-exchange with ZnS quantum dots. Sens Actuators B Chem. 2018 Jan 1;254:910–5.

17.   Guidelli EJ, Lignos I, Yoo JJ, Lusardi M, Baffa O, Jensen KF. Mechanistic insights and controlled synthesis of radioluminescent ZnSe quantum dots using a microfluidic reactor. :7.

18.   Xing X, Wang D, Chen Z, Zheng B, Li B, Wu D. ZnTe quantum dots as fluorescence sensors for the detection of iron ions. J Mater Sci Mater Electron. 2018 Aug 1;29(16):14192–9.

19.   Wang L, Xu D, Gao J, Chen X, Duo Y, Zhang H. Semiconducting quantum dots: Modification and applications in biomedical science. Sci China Mater. 2020 Sep;63(9):1631–50.

20.   Yuan Q, Hein S, Misra RDK. New generation of chitosan-encapsulated ZnO quantum dots loaded with drug: Synthesis, characterization and in vitro drug delivery response. Acta Biomater. 2010 Jul 1;6(7):2732–9.

21.   Zhou R, Zhao Q, Liu K-K, Lu Y-J, Dong L, Shan C-X. Europium-decorated ZnO quantum dots as a fluorescent sensor for the detection of an anthrax biomarker. J Mater Chem C. 2017 Feb 16;5(7):1685–91.

22.   Gao X, Cui Y, Levenson RM, Chung LWK, Nie S. In vivo cancer targeting and imaging with semiconductor quantum dots. Nat Biotechnol. 2004 Aug;22(8):969–76.

23.   Lee J, Sundar VC, Heine JR, Bawendi MG, Jensen KF. Full Color Emission from II-VI Semiconductor Quantum Dot-Polymer Composites. :4.

24.   Villamena FA. Chapter 4 - Fluorescence Technique. In: Villamena FA, editor. Reactive Species Detection in Biology [Internet]. Boston: Elsevier; 2017 [cited 2021 Mar 25]. p. 87–162. Available from: https://www.sciencedirect.com/science/article/pii/B9780124200173000037

25.   Bang E, Choi Y, Cho J, Suh Y-H, Ban HW, Son JS, et al. Large-Scale Synthesis of Highly Luminescent InP@ZnS Quantum Dots Using Elemental Phosphorus Precursor. Chem Mater. 2017 May 23;29(10):4236–43.

26.   Chandrasekaran V, Tessier MD, Dupont D, Geiregat P, Hens Z, Brainis E. Nearly Blinking-Free, High-Purity Single-Photon Emission by Colloidal InP/ZnSe Quantum Dots. Nano Lett. 2017 Oct 11;17(10):6104–9.

27.   Ren Z, Sun J, Li H, Mao P, Wei Y, Zhong X, et al. Bilayer PbS Quantum Dots for High-Performance Photodetectors. Adv Mater. 2017;29(33):1702055.

28.   Yan L, Shen X, Zhang Y, Zhang T, Zhang X, Feng Y, et al. Near-infrared light emitting diodes using PbSe quantum dots. RSC Adv. 2015 Jun 18;5(67):54109–14.

29.   Gao S, Wang B, Liu X, Guo Z, Liu Z, Wang Y. PbTe quantum dots as electron transfer intermediates for the enhanced hydrogen evolution reaction of amorphous MoSx/TiO2 nanotube arrays. Nanoscale. 2018 May 31;10(21):10288–95.

30.   Davis NJLK, Böhm ML, Tabachnyk M, Wisnivesky-Rocca-Rivarola F, Jellicoe TC, Ducati C, et al. Multiple-exciton generation in lead selenide nanorod solar cells with external quantum efficiencies exceeding 120%. Nat Commun. 2015 Sep 28;6(1):8259.

31.   Sun Y-P, Zhou B, Lin Y, Wang W, Fernando KAS, Pathak P, et al. Quantum-Sized Carbon Dots for Bright and Colorful Photoluminescence. J Am Chem Soc. 2006 Jun 1;128(24):7756–7.

32.   Cheng X, Lowe SB, Reece PJ, Gooding JJ. Colloidal silicon quantum dots: from preparation to the modification of self-assembled monolayers (SAMs) for bio-applications. Chem Soc Rev. 2014 Mar 24;43(8):2680–700.

33.   Ponomarenko LA, Schedin F, Katsnelson MI, Yang R, Hill EW, Novoselov KS, et al. Chaotic Dirac Billiard in Graphene Quantum Dots. Science. 2008 Apr 18;320(5874):356–8.

34.   Gui R, Jin H, Wang Z, Li J. Black phosphorus quantum dots: synthesis, properties, functionalized modification and applications. Chem Soc Rev. 2018 Aug 28;47(17):6795–823.

35.   Luo M, Fan T, Zhou Y, Zhang H, Mei L. 2D Black Phosphorus–Based Biomedical Applications. Adv Funct Mater. 2019 Mar;29(13):1808306.

36.   Sun Z, Zhao Y, Li Z, Cui H, Zhou Y, Li W, et al. TiL4-Coordinated Black Phosphorus Quantum Dots as an Efficient Contrast Agent for In Vivo Photoacoustic Imaging of Cancer. Small. 2017;13(11):1602896.

37.   Fan T, Zhou Y, Qiu M, Zhang H. Black phosphorus: A novel nanoplatform with potential in the field of bio-photonic nanomedicine. J Innov Opt Health Sci. 2018 Oct 26;11(06):1830003.

38.   Ponraj JS, Xu Z-Q, Dhanabalan SC, Mu H, Wang Y, Yuan J, et al. Photonics and optoelectronics of two-dimensional materials beyond graphene. Nanotechnology. 2016 Oct;27(46):462001.

39.   Song YF, Zhang H, Zhao LM, Shen DY, Tang DY. Coexistence and interaction of vector and bound vector solitons in a dispersion-managed fiber laser mode locked by graphene. Opt Express. 2016 Jan 25;24(2):1814–22.

40.   Allen PM, Bawendi MG. Ternary I−III−VI Quantum Dots Luminescent in the Red to Near-Infrared. J Am Chem Soc. 2008 Jul 1;130(29):9240–1.

41.   Li D-M, Cheng L-Y, Zhang Y-D, Zhang Q-X, Huang X-M, Luo Y-H, et al. Development of Cu2S/carbon composite electrode for CdS/CdSe quantum dot sensitized solar cell modules. Sol Energy Mater Sol Cells. 2014 Jan;120:454–61.

42.   Li S-L, Yang Q-Q, Liu X-Y, Jiang F-L, Xiong J, Jiang P, et al. Zn-doped Cu2S quantum dots as new high-efficiency inhibitors against human insulin fibrillation based on specific electrostatic interaction with oligomers. Int J Biol Macromol. 2021 May 15;179:161–9.

43.   Zimmer JP, Kim S-W, Ohnishi S, Tanaka E, Frangioni JV, Bawendi MG. Size Series of Small Indium Arsenide−Zinc Selenide Core−Shell Nanocrystals and Their Application to In Vivo Imaging. J Am Chem Soc. 2006 Mar 1;128(8):2526–7.

44.   Du C-F, You T, Jiang L, Yang S-Q, Zou K, Han K-L, et al. Controllable synthesis of ultrasmall CuInSe2 quantum dots for photovoltaic application. RSC Adv. 2014 Aug 4;4(64):33855–60.

45.   Jara DH, Yoon SJ, Stamplecoskie KG, Kamat PV. Size-Dependent Photovoltaic Performance of CuInS2 Quantum Dot-Sensitized Solar Cells. Chem Mater. 2014 Dec 23;26(24):7221–8.

46.   Panthani MG, Khan TA, Reid DK, Hellebusch DJ, Rasch MR, Maynard JA, et al. In Vivo Whole Animal Fluorescence Imaging of a Microparticle-Based Oral Vaccine Containing (CuInSexS2–x)/ZnS Core/Shell Quantum Dots. Nano Lett. 2013 Sep 11;13(9):4294–8.

47.   Zhou X, Liang H, Jiang P, Zhang KY, Liu S, Yang T, et al. Multifunctional Phosphorescent Conjugated Polymer Dots for Hypoxia Imaging and Photodynamic Therapy of Cancer Cells. Adv Sci. 2016;3(2):1500155.

48.   Wu C, Hansen SJ, Hou Q, Yu J, Zeigler M, Jin Y, et al. Design of Highly Emissive Polymer Dot Bioconjugates for in vivo Tumor Targeting. Angew Chem Int Ed Engl. 2011 Apr 4;50(15):3430–4.

49.   Wu C, Schneider T, Zeigler M, Yu J, Schiro PG, Burnham DR, et al. Bioconjugation of ultrabright semiconducting polymer dots for specific cellular targeting. J Am Chem Soc. 2010 Nov 3;132(43):15410–7.

50.   Sun W, Yu J, Deng R, Rong Y, Fujimoto B, Wu C, et al. Semiconducting Polymer Dots Doped with Europium Complexes Showing Ultranarrow Emission and Long Luminescence Lifetime for Time-Gated Cellular Imaging. Angew Chem Int Ed. 2013;52(43):11294–7.

51.   Liu D, Zhang X, Zhao J, Chen S, Yuan R. An ultrasensitive sensing platform for microRNA-155 based on H2O2 quenched hydroxide-dependent ECL emission of PFO Pdots. Biosens Bioelectron. 2020 Feb 15;150:111872.

52.   Pecher J, Mecking S. Nanoparticles of conjugated polymers. Chem Rev. 2010 Oct 13;110(10):6260–79.

53.   Kaeser A, Schenning APHJ. Fluorescent nanoparticles based on self-assembled pi-conjugated systems. Adv Mater Deerfield Beach Fla. 2010 Jul 27;22(28):2985–97.

54.   Mohanty B, Ghorbani-Asl M, Kretschmer S, Ghosh A, Guha P, Panda SK, et al. MoS2 Quantum Dots as Efficient Catalyst Materials for the Oxygen Evolution Reaction. ACS Catal. 2018 Mar 2;8(3):1683–9.

55.   Zhao M, Chen A-Y, Huang D, Chai Y-Q, Zhuo Y, Yuan R. MoS2 Quantum Dots as New Electrochemiluminescence Emitters for Ultrasensitive Bioanalysis of Lipopolysaccharide. Anal Chem. 2017 Aug 15;89(16):8335–42.

56.   Wang J, Tan X, Pang X, Liu L, Tan F, Li N. MoS2 Quantum Dot@Polyaniline Inorganic–Organic Nanohybrids for in Vivo Dual-Modal Imaging Guided Synergistic Photothermal/Radiation Therapy. ACS Appl Mater Interfaces. 2016 Sep 21;8(37):24331–8.

57.   Shein I, Ivanovskii A. Graphene-like nanocarbides and nanonitrides of d metals (MXenes): Synthesis, properties and simulation. Micro Nano Lett IET. 2013 Feb 1;8:59–62.

58.   Lei J-C, Zhang X, Zhou Z. Recent advances in MXene: Preparation, properties, and applications. Front Phys. 2015 Jun;10(3):276–86.

59.   Barsoum M. MAX phases: Properties of machinable ternary carbides and nitrides. MAX Phases: Properties of Machinable Ternary Carbides and Nitrides. 2013. 1 p.

60.   Zha X-H, Yin J, Zhou Y, Huang Q, Luo K, Lang J, et al. Intrinsic Structural, Electrical, Thermal, and Mechanical Properties of the Promising Conductor Mo2C MXene. J Phys Chem C. 2016 Jul 21;120(28):15082–8.

61.   Shi C, Beidaghi M, Naguib M, Mashtalir O, Gogotsi Y, Billinge SJL. Structure of Nanocrystalline ${\mathrm{Ti}}_{3}{\mathrm{C}}_{2}$ MXene Using Atomic Pair Distribution Function. Phys Rev Lett. 2014 Mar 26;112(12):125501.

62.   Liu F, Zhou J, Wang S, Wang B, Shen C, Wang L, et al. Preparation of High-Purity V2C MXene and Electrochemical Properties as Li-Ion Batteries. J Electrochem Soc. 2017 Feb 4;164(4):A709.

63.   Mashtalir O, Lukatskaya MR, Zhao M-Q, Barsoum MW, Gogotsi Y. Amine-Assisted Delamination of Nb2C MXene for Li-Ion Energy Storage Devices. Adv Mater. 2015;27(23):3501–6.

64.   Enyashin AN, Ivanovskii AL. Structural and Electronic Properties and Stability of MXenes Ti2C and Ti3C2 Functionalized by Methoxy Groups. J Phys Chem C. 2013 Jul 3;117(26):13637–43.

65.   Zhao S, Meng X, Zhu K, Du F, Chen G, Wei Y, et al. Li-ion uptake and increase in interlayer spacing of Nb4C3 MXene. Energy Storage Mater. 2017 Jul 1;8:42–8.

66.   Zhu J, Ha E, Zhao G, Zhou Y, Huang D, Yue G, et al. Recent advance in MXenes: A promising 2D material for catalysis, sensor and chemical adsorption. Coord Chem Rev. 2017 Dec;352:306–27.

67.   Sinha A, Dhanjai, Zhao H, Huang Y, Lu X, Chen J, et al. MXene: An emerging material for sensing and biosensing. TrAC Trends Anal Chem. 2018 Aug 1;105:424–35.

68.   Yu X, Cai X, Cui H, Lee S-W, Yu X-F, Liu B. Fluorine-free preparation of titanium carbide MXene quantum dots with high near-infrared photothermal performances for cancer therapy. Nanoscale. 2017 Nov 23;9(45):17859–64.

69.   Guo Z, Zhu X, Wang S, Lei C, Huang Y, Nie Z, et al. Fluorescent Ti3C2 MXene quantum dots for an alkaline phosphatase assay and embryonic stem cell identification based on the inner filter effect. Nanoscale. 2018 Oct 25;10(41):19579–85.

70.   Lu S, Sui L, Liu Y, Yong X, Xiao G, Yuan K, et al. White Photoluminescent Ti3C2 MXene Quantum Dots with Two-Photon Fluorescence. Adv Sci. 2019;6(9):1801470.

71.   Xu G, Niu Y, Yang X, Jin Z, Wang Y, Xu Y, et al. Preparation of Ti3C2Tx MXene-Derived Quantum Dots with White/Blue-Emitting Photoluminescence and Electrochemiluminescence. Adv Opt Mater. 2018;6(24):1800951.

72.   Xue Q, Zhang H, Zhu M, Pei Z, Li H, Wang Z, et al. Photoluminescent Ti3C2 MXene Quantum Dots for Multicolor Cellular Imaging. Adv Mater. 2017;29(15):1604847.

73.   Song J, Li J, Li X, Xu L, Dong Y, Zeng H. Quantum Dot Light-Emitting Diodes Based on Inorganic Perovskite Cesium Lead Halides (CsPbX3). Adv Mater. 2015;27(44):7162–7.

74.   Wang Y, Li X, Song J, Xiao L, Zeng H, Sun H. All-Inorganic Colloidal Perovskite Quantum Dots: A New Class of Lasing Materials with Favorable Characteristics. Adv Mater. 2015;27(44):7101–8.

75.   Wang H, Kim DH. Perovskite-based photodetectors: materials and devices. Chem Soc Rev. 2017 Aug 29;46(17):5204–36.

76.   Im J-H, Lee C-R, Lee J-W, Park S-W, Park N-G. 6.5% efficient perovskite quantum-dot-sensitized solar cell. Nanoscale. 2011 Oct 5;3(10):4088–93.

77.   Reshma VG, Mohanan PV. Quantum dots: Applications and safety consequences. J Lumin. 2019 Jan 1;205:287–98.

78.   Fendler JH. Nanoparticles and Nanostructured Films: Preparation, Characterization, and Applications. John Wiley & Sons; 2008. 491 p.

79.   Xia Y, Whitesides GM. Soft Lithography. Angew Chem Int Ed Engl. 1998 Mar 16;37(5):550–75.

80.   Crozier PA, Tolle J, Kouvetakis J, Ritter C. Synthesis of uniform GaN quantum dot arrays via electron nanolithography of D2GaN3. Appl Phys Lett. 2004 Apr 23;84(18):3441–3.

81.   Teo BK, Sun XH. From Top-Down to Bottom-Up to Hybrid Nanotechnologies: Road to Nanodevices. J Clust Sci. 2006 Dec 1;17(4):529–40.

82.   Chang LL, Ploog K, editors. Molecular Beam Epitaxy and Heterostructures [Internet]. Springer Netherlands; 1985 [cited 2021 Mar 28]. (Nato Science Series E:). Available from: https://www.springer.com/gp/book/9789024731183

83.   Arthur JR. Molecular beam epitaxy. Surf Sci. 2002 Mar 10;500(1):189–217.

84.   Alchalabi K, Zimin D, Kostorz G, Zogg H. Self-Assembled Semiconductor Quantum Dots with Nearly Uniform Sizes. Phys Rev Lett. 2003 Jan 17;90(2):026104.

85.   Yu Y, Zhang K, Sun S. One-pot aqueous synthesis of near infrared emitting PbS quantum dots. Appl Surf Sci. 2012 Jul 1;258(18):7181–7.

86.   Y Z, Z L, M C, Hm C, Gq L, Zp X. One-pot preparation of highly fluorescent cadmium telluride/cadmium sulfide quantum dots under neutral-pH condition for biological applications. J Colloid Interface Sci. 2012 Oct 2;390(1):3–10.

87.   Brichkin SB, Razumov VF. Colloidal quantum dots: synthesis, properties and applications. Russ Chem Rev. 2016 Dec 1;85(12):1297.

88.   Narayanan KB, Sakthivel N. Biological synthesis of metal nanoparticles by microbes. Adv Colloid Interface Sci. 2010 Apr;156(1–2):1–13.

89.   Suslick KS, Price GJ. Applications of ultrasound to materials chemistry. Annu Rev Mater Sci. 1999 Aug 1;29(1):295–326.

90.   Shchukin DG, Radziuk D, Möhwald H. Ultrasonic Fabrication of Metallic Nanomaterials and Nanoalloys. Annu Rev Mater Res. 2010 Aug 1;40:345–62.

91.   Xu H, Zeiger BW, Suslick KS. Sonochemical synthesis of nanomaterials. Chem Soc Rev. 2013 Mar 11;42(7):2555–67.

92.   Hinman JJ, Suslick KS. Nanostructured Materials Synthesis Using Ultrasound. Top Curr Chem. 2017 Feb;375(1):12.

93.   Suslick KS, Flannigan DJ. Inside a Collapsing Bubble: Sonoluminescence and the Conditions During Cavitation. Annu Rev Phys Chem. 2008 Apr 4;59(1):659–83.

94.   Flannigan DJ, Suslick KS. Plasma formation and temperature measurement during single-bubble cavitation. Nature. 2005 Mar;434(7029):52–5.

95.   Didenko YT, Suslick KS. The energy efficiency of formation of photons, radicals and ions during single-bubble cavitation. Nature. 2002 Jul;418(6896):394–7.

96.   Flint EB, Suslick KS. The Temperature of Cavitation. Science. 1991 Sep 20;253(5026):1397–9.

97.   Ouerhani T, Pflieger R, Ben Messaoud W, Nikitenko SI. Spectroscopy of Sonoluminescence and Sonochemistry in Water Saturated with N2–Ar Mixtures. J Phys Chem B. 2015 Dec 31;119(52):15885–91.

98.   Riesz P, Berdahl D, Christman C. Free Radical Generation by Ultrasound in Aqueous and Nonaqueous Solutions. Environ Health Perspect. 1986 Jan 1;64:233–52.

99.   Makino K, Mossoba MM, Riesz P. Chemical effects of ultrasound on aqueous solutions. Evidence for hydroxyl and hydrogen free radicals (.cntdot.OH and .cntdot.H) by spin trapping. J Am Chem Soc. 1982 Jun 1;104(12):3537–9.

100.   Gharat NN, Rathod VK. Chapter 1 - Ultrasound-assisted organic synthesis. In: Inamuddin, Boddula R, Asiri AM, editors. Green Sustainable Process for Chemical and Environmental Engineering and Science [Internet]. Elsevier; 2020 [cited 2021 Mar 29]. p. 1–41. Available from: https://www.sciencedirect.com/science/article/pii/B9780128195406000012

101.   Suslick KS, Choe SB, Cichowlas AA, Grinstaff MW. Sonochemical synthesis of amorphous iron. Nature. 1991 Jan 1;353(6343):414–6.

102.   Ohayon E, Gedanken A. The application of ultrasound radiation to the synthesis of nanocrystalline metal oxide in a non-aqueous solvent. Ultrason Sonochem. 2010 Jan 1;17(1):173–8.

103.   Flannigan DJ, Hopkins SD, Suslick KS. Sonochemistry and sonoluminescence in ionic liquids, molten salts, and concentrated electrolyte solutions. J Organomet Chem. 2005 Aug 1;690(15):3513–7.

104.   Oxley JD, Prozorov T, Suslick KS. Sonochemistry and Sonoluminescence of Room-Temperature Ionic Liquids. J Am Chem Soc. 2003 Sep 1;125(37):11138–9.

105.   Suslick KS, Fang M, Hyeon T. Sonochemical Synthesis of Iron Colloids. J Am Chem Soc. 1996 Jan 1;118(47):11960–1.

106.   Bang JH, Suslick KS. Sonochemical Synthesis of Nanosized Hollow Hematite. J Am Chem Soc. 2007 Feb 1;129(8):2242–3.

107.   Dhas NA, Suslick KS. Sonochemical Preparation of Hollow Nanospheres and Hollow Nanocrystals. J Am Chem Soc. 2005 Mar 1;127(8):2368–9.

108.   Baigent CL, Müller G. A colloidal gold prepared with ultrasonics. Experientia. 1980 Apr 1;36(4):472–3.

109.   Okitsu K, Ashokkumar M, Grieser F. Sonochemical Synthesis of Gold Nanoparticles: Effects of Ultrasound Frequency. J Phys Chem B. 2005 Nov;109(44):20673–5.

110.   Yeung SA, Hobson R, Biggs S, Grieser F. Formation of gold sols using ultrasound. J Chem Soc Chem Commun. 1993 Jan 1;(4):378–9.

111.   Okitsu K, Yue A, Tanabe S, Matsumoto H, Yobiko Y, Yoo Y. Sonolytic Control of Rate of Gold(III) Reduction and Size of Formed Gold Nanoparticles: Relation between Reduction Rates and Sizes of Formed Nanoparticles. Bull Chem Soc Jpn. 2002 Oct 1;75(10):2289–96.

112.   Caruso RA, Ashokkumar M, Grieser F. Sonochemical Formation of Gold Sols. Langmuir. 2002 Oct 1;18(21):7831–6.

113.   Nagata Y, Mizukoshi Y, Okitsu K, Maeda Y. Sonochemical formation of gold particles in aqueous solution. Radiat Res. 1996 Sep;146(3):333–8.

114.   Beckett MA, Hua I. Impact of Ultrasonic Frequency on Aqueous Sonoluminescence and Sonochemistry. J Phys Chem A. 2001 Apr 1;105(15):3796–802.

115.   Okitsu K, Sharyo K, Nishimura R. One-Pot Synthesis of Gold Nanorods by Ultrasonic Irradiation: The Effect of pH on the Shape of the Gold Nanorods and Nanoparticles. Langmuir. 2009 Jul 21;25(14):7786–90.

116.   Zhang J, Du J, Han B, Liu Z, Jiang T, Zhang Z. Sonochemical Formation of Single-Crystalline Gold Nanobelts. Angew Chem Int Ed. 2006;45(7):1116–9.

117.   Sánchez-Iglesias A, Pastoriza-Santos I, Pérez-Juste J, Rodríguez-González B, García de Abajo FJ, Liz-Marzán LM. Synthesis and Optical Properties of Gold Nanodecahedra with Size Control. Adv Mater. 2006;18(19):2529–34.

118.   Jiang L-P, Xu S, Zhu J-M, Zhang J-R, Zhu J-J, Chen H-Y. Ultrasonic-assisted synthesis of monodisperse single-crystalline silver nanoplates and gold nanorings. Inorg Chem. 2004 Sep 20;43(19):5877–83.

119.   Gümeci C, Cearnaigh DU, Casadonte DJ, Korzeniewski C. Synthesis of PtCu3 bimetallic nanoparticles as oxygen reduction catalysts via a sonochemical method. J Mater Chem A. 2013 Jan 17;1(6):2322–30.

120.   Godínez-García A, Pérez-Robles JF, Martínez-Tejada HV, Solorza-Feria O. Characterization and electrocatalytic properties of sonochemical synthesized PdAg nanoparticles. Mater Chem Phys. 2012 Jun 15;134(2):1013–9.

121.   Matin MdA, Jang J-H, Kwon Y-U. PdM nanoparticles (M = Ni, Co, Fe, Mn) with high activity and stability in formic acid oxidation synthesized by sonochemical reactions. J Power Sources. 2014 Sep 15;262:356–63.

122.   Xu H, Suslick KS. Sonochemical Synthesis of Highly Fluorescent Ag Nanoclusters. ACS Nano. 2010 Jun 22;4(6):3209–14.

123.   Petty JT, Zheng J, Hud NV, Dickson RM. DNA-Templated Ag Nanocluster Formation. J Am Chem Soc. 2004 Apr 28;126(16):5207–12.

124.   Zheng J, Dickson RM. Individual water-soluble dendrimer-encapsulated silver nanodot fluorescence. J Am Chem Soc. 2002 Nov 27;124(47):13982–3.

125.   Zhang J, Xu S, Kumacheva E. Photogeneration of Fluorescent Silver Nanoclusters in Polymer Microgels. Adv Mater. 2005;17(19):2336–40.

126.   Gwinn EG, O'Neill P, Guerrero AJ, Bouwmeester D, Fygenson DK. Sequence-Dependent Fluorescence of DNA-Hosted Silver Nanoclusters. Adv Mater. 2008;20(2):279–83.

127.   Vabbina PK, Kaushik A, Pokhrel N, Bhansali S, Pala N. Electrochemical cortisol immunosensors based on sonochemically synthesized zinc oxide 1D nanorods and 2D nanoflakes. Biosens Bioelectron. 2015 Jan 15;63:124–30.

128.   Singh G, Joyce EM, Beddow J, Mason TJ. EVALUATION OF ANTIBACTERIAL ACTIVITY OF ZnO NANOPARTICLES COATED SONOCHEMICALLY ONTO TEXTILE FABRICS. 2012;15.

129.   Gottesman R, Shukla S, Perkas N, Solovyov LA, Nitzan Y, Gedanken A. Sonochemical Coating of Paper by Microbiocidal Silver Nanoparticles. Langmuir. 2011 Jan 18;27(2):720–6.

130.   Abramova A, Gedanken A, Popov V, Ooi EH, Mason T, Joyce E, et al. A sonochemical technology for coating of textiles with antibacterial nanoparticles and equipment for its implementation. Mater Lett. 2012 Jan 1;96:121–4.

131.   Prozorov T, Prozorov R, Suslick KS. High Velocity Interparticle Collisions Driven by Ultrasound. J Am Chem Soc. 2004 Nov 1;126(43):13890–1.

132.   Doktycz SJ, Suslick KS. Interparticle collisions driven by ultrasound. Science. 1990 Mar 2;247(4946):1067–9.

133.   Suslick KS. Sonochemistry. Science. 1990 Mar 23;247(4949):1439–45.

134.   Shi Y, Zhu C, Wang L, Zhao C, Li W, Fung KK, et al. Ultrarapid Sonochemical Synthesis of ZnO Hierarchical Structures: From Fundamental Research to High Efficiencies up to 6.42% for Quasi-Solid Dye-Sensitized Solar Cells. Chem Mater. 2013 Mar 26;25(6):1000–12.

135.   Zhang Q, Cao G. Nanostructured photoelectrodes for dye-sensitized solar cells. Nano Today. 2011 Feb;6(1):91–109.

136.   Memarian N, Concina I, Braga A, Rozati SM, Vomiero A, Sberveglieri G. Hierarchically assembled ZnO nanocrystallites for high-efficiency dye-sensitized solar cells. Angew Chem Int Ed Engl. 2011 Dec 16;50(51):12321–5.

137.   Baxter J, Walker A, Ommering K, Aydil E. Synthesis and Characterization of ZnO Nanowires and Their Integration into Dye-Sensitized Solar Cells. Nanotechnol Nanotechnol. 2006 Jun 14;17:304–12.

138.   Benkstein KD, Kopidakis N, van de Lagemaat J, Frank AJ. Influence of the Percolation Network Geometry on Electron Transport in Dye-Sensitized Titanium Dioxide Solar Cells. J Phys Chem B. 2003 Aug 1;107(31):7759–67.

139.   Zhou X, Liu G, Yu J, Fan W. Surface plasmon resonance-mediated photocatalysis by noble metal-based composites under visible light. J Mater Chem. 2012 Sep 25;22(40):21337–54.

140.   Ueno S, Fujihara S. Effective Sol-Gel Nanocoatings on ZnO Electrodes for Suppressing Recombination in Dye-Sensitized Solar Cells. Int J Photoenergy. 2012 Jun 11;2012:e268173.

141.   Shi Y, Zhu C, Wang Y, Wang L, Du Y, Gu J, et al. A green route and rational design for ZnO-based high-efficiency photovoltaics. Nanoscale. 2014 Apr 10;6.

142.   Lu H, Wang S, Zhao L, Li J, Dong B, Xu Z. Hierarchical ZnO microarchitectures assembled by ultrathin nanosheets: hydrothermal synthesis and enhanced photocatalytic activity. J Mater Chem. 2011 Mar 8;21(12):4228–34.

143.   Li X, Li X, Zhu B, Wang J, Lan H, Chen X. Synthesis of porous ZnS, ZnO and ZnS/ZnO nanosheets and their photocatalytic properties. RSC Adv. 2017 Jun 13;7(49):30956–62.

144.   Xu L, Chen Q, Xu D. Hierarchical ZnO Nanostructures Obtained by Electrodeposition. J Phys Chem C. 2007 Aug 1;111(31):11560–5.

145.   Zhu C, Shi Y, Cheng C, Wang L, Fung KK, Wang N. Correlation between the morphology and performance enhancement of ZnO hierarchical flower photoanodes in quasi-solid dye-sensitized solar cells. J Nanomater. 2012 Jan 1;2012:4:4.

146.   Mahmood K, Khalid A, Mehran T. Nanostructured ZnO electron transporting materials for hysteresis-free perovskite solar cells. Sol Energy. 2018 Oct 1;173.

147.   Lang RJ. Ultrasonic Atomization of Liquids. J Acoust Soc Am. 1962 Jan 1;34(1):6–8.

148.   Bang JH, Suslick KS. Applications of Ultrasound to the Synthesis of Nanostructured Materials. Adv Mater. 2010;22(10):1039–59.

149.   Okuyama K, Wuled Lenggoro I. Preparation of nanoparticles via spray route. Chem Eng Sci. 2003 Feb 1;58(3):537–47.

150.   Messing GL, Zhang S-C -C, Jayanthi GV. Ceramic Powder Synthesis by Spray Pyrolysis. J Am Ceram Soc. 1993 Nov;76(11):2707–26.

151.   Richards WT, Loomis AL. THE CHEMICAL EFFECTS OF HIGH FREQUENCY SOUND WAVES I. A PRELIMINARY SURVEY. J Am Chem Soc. 1927 Dec 1;49(12):3086–100.

152.   Kapustin AP. The Effects of Ultrasound on the Kinetics of Crystallization [Internet]. Springer US; 1963 [cited 2021 Apr 10]. Available from: https://www.springer.com/gp/book/9781468415506

153.   Principe JR, Skauen DM. Preparation of Microcrystalline Progesterone Using Ultrasound. J Pharm Sci. 1962 Apr 1;51(4):389–90.

154.   Cohn RM, Skauen DM. Controlled Crystallization of Hydrocortisone by Ultrasonic Irradiation. J Pharm Sci. 1964 Sep 1;53(9):1040–5.

155.   Skauen DM. Some pharmaceutical applications of ultrasonics. J Pharm Sci. 1967 Nov 1;56(11):1373–85.

156.   Hem SL. The effect of ultrasonic vibrations on crystallization processes. Ultrasonics. 1967 Oct 1;5(4):202–7.

157.   Li H, Wang J, Bao Y, Guo Z, Zhang M. Rapid sonocrystallization in the salting-out process. J Cryst Growth. 2003 Jan 1;247(1):192–8.

158.   Guo Z, Zhang M, Li H, Wang J, Kougoulos E. Effect of ultrasound on anti-solvent crystallization process. J Cryst Growth. 2005 Jan 3;273(3):555–63.

159.   Kurotani M, Miyasaka E, Ebihara S, Hirasawa I. Effect of ultrasonic irradiation on the behavior of primary nucleation of amino acids in supersaturated solutions. J Cryst Growth. 2009 Apr 15;311(9):2714–21.

160.   Zeiger BW, Suslick KS. Sonofragmentation of Molecular Crystals. J Am Chem Soc. 2011 Sep 21;133(37):14530–3.

161.   Guo Y, Li J. MoS2 quantum dots: synthesis, properties and biological applications. Mater Sci Eng C. 2020 Apr;109:110511.

162.   Wang Y, Ni Y. Molybdenum Disulfide Quantum Dots as a Photoluminescence Sensing Platform for 2,4,6-Trinitrophenol Detection. Anal Chem. 2014 Aug 5;86(15):7463–70.

163.   Dai W, Dong H, Fugetsu B, Cao Y, Lu H, Ma X, et al. Tunable Fabrication of Molybdenum Disulfide Quantum Dots for Intracellular MicroRNA Detection and Multiphoton Bioimaging. Small. 2015;11(33):4158–64.

164.   Zhou K, Zhang Y, Xia Z, Wei W. As-prepared MoS2 quantum dot as a facile fluorescent probe for long-term tracing of live cells. Nanotechnology. 2016 Jul 8;27(27):275101.

165.   Li BL, Chen LX, Zou HL, Lei JL, Luo HQ, Li NB. Electrochemically induced Fenton reaction of few-layer MoS2 nanosheets: preparation of luminescent quantum dots via a transition of nanoporous morphology. Nanoscale. 2014 Jul 24;6(16):9831–8.

166.   Gopalakrishnan D, Damien D, Li B, Gullappalli H, Pillai VK, Ajayan PM, et al. Electrochemical synthesis of luminescent MoS2 quantum dots. Chem Commun. 2015 Mar 26;51(29):6293–6.

167.   Wang N, Wei F, Qi Y, Li H, Lu X, Zhao G, et al. Synthesis of Strongly Fluorescent Molybdenum Disulfide Nanosheets for Cell-Targeted Labeling. ACS Appl Mater Interfaces. 2014 Nov 26;6(22):19888–94.

168.   Liu Q, Hu C, Wang X. A facile one-step method to produce MoS2 quantum dots as promising bio-imaging materials. RSC Adv. 2016 Mar 4;6(30):25605–10.

169.   Park SJ, Pak SW, Qiu D, Kang JH, Song DY, Kim EK. Structural and optical characterization of MoS2 quantum dots defined by thermal annealing. J Lumin. 2017 Mar 1;183:62–7.

170.   Siddiqui GU, Ali J, Choi KH, Jang Y, Lee K. Fabrication of blue luminescent MoS2 quantum dots by wet grinding assisted co-solvent sonication. J Lumin. 2016 Jan;169:342–7.

171.   Gu W, Yan Y, Cao X, Zhang C, Ding C, Xian Y. A facile and one-step ethanol-thermal synthesis of MoS2 quantum dots for two-photon fluorescence imaging. J Mater Chem B. 2015 Dec 17;4(1):27–31.

172.   Zhou K-G, Mao N-N, Wang H-X, Peng Y, Zhang H-L. A Mixed-Solvent Strategy for Efficient Exfoliation of Inorganic Graphene Analogues. Angew Chem Int Ed. 2011;50(46):10839–42.

173.   Smith RJ, King PJ, Lotya M, Wirtz C, Khan U, De S, et al. Large-scale exfoliation of inorganic layered compounds in aqueous surfactant solutions. Adv Mater Deerfield Beach Fla. 2011 Sep 8;23(34):3944–8.

174.   Štengl V, Henych J. Strongly luminescent monolayered MoS2 prepared by effective ultrasound exfoliation. Nanoscale. 2013;5(8):3387.

175.   Wu J-Y, Zhang X-Y, Ma X-D, Qiu Y-P, Zhang T. High quantum-yield luminescent MoS2 quantum dots with variable light emission created via direct ultrasonic exfoliation of MoS2 nanosheets. RSC Adv. 2015 Nov 3;5(115):95178–82.

176.   Qiao W, Yan S, Song X, Zhang X, He X, Zhong W, et al. Luminescent monolayer MoS2 quantum dots produced by multi-exfoliation based on lithium intercalation. Appl Surf Sci. 2015 Dec 1;359:130–6.

177.   Xu S, Li D, Wu P. One-Pot, Facile, and Versatile Synthesis of Monolayer MoS2/WS2 Quantum Dots as Bioimaging Probes and Efficient Electrocatalysts for Hydrogen Evolution Reaction. Adv Funct Mater. 2015;25(7):1127–36.

178.   Wang X, Wu Q, Jiang K, Wang C, Zhang C. One-step synthesis of water-soluble and highly fluorescent MoS2 quantum dots for detection of hydrogen peroxide and glucose. Sens Actuators B Chem. 2017 Nov 1;252:183–90.

179.   Ren X, Pang L, Zhang Y, Ren X, Fan H, Liu S (Frank). One-step hydrothermal synthesis of monolayer MoS2 quantum dots for highly efficient electrocatalytic hydrogen evolution. J Mater Chem A. 2015 May 12;3(20):10693–7.

180.   Wang Y, Hu J, Zhuang Q, Ni Y. Label-Free Fluorescence Sensing of Lead(II) Ions and Sulfide Ions Based on Luminescent Molybdenum Disulfide Nanosheets. ACS Sustain Chem Eng. 2016 May 2;4(5):2535–41.

181.   Xu B, Su Y, Li L, Liu R, Lv Y. Thiol-functionalized single-layered MoS2 nanosheet as a photoluminescence sensing platform via charge transfer for dopamine detection. Sens Actuators B Chem. 2017 Jul 1;246:380–8.

182.   Haldar D, Dinda D, Saha SK. High selectivity in water soluble MoS2 quantum dots for sensing nitro explosives. J Mater Chem C. 2016 Jun 30;4(26):6321–6.

183.   Huang H, Du C, Shi H, Feng X, Li J, Tan Y, et al. Water-Soluble Monolayer Molybdenum Disulfide Quantum Dots with Upconversion Fluorescence. Part Part Syst Charact. 2015;32(1):72–9.

184.   Gu W, Yan Y, Zhang C, Ding C, Xian Y. One-Step Synthesis of Water-Soluble MoS2 Quantum Dots via a Hydrothermal Method as a Fluorescent Probe for Hyaluronidase Detection. ACS Appl Mater Interfaces. 2016 May 11;8(18):11272–9.

185.   Lin H, Wang C, Wu J, Xu Z, Huang Y, Zhang C. Colloidal synthesis of MoS2 quantum dots: size-dependent tunable photoluminescence and bioimaging. New J Chem. 2015 Oct 29;39(11):8492–7.

186.   Kumar R, Kumar VB, Gedanken A. Sonochemical synthesis of carbon dots, mechanism, effect of parameters, and catalytic, energy, biomedical and tissue engineering applications. Ultrason Sonochem. 2020 Jun;64:105009.

187.   Li H, He X, Liu Y, Huang H, Lian S, Lee S-T, et al. One-step ultrasonic synthesis of water-soluble carbon nanoparticles with excellent photoluminescent properties. Carbon. 2011;49(2):605–9.

188.   Wei K, Li J, Ge Z, You Y, Xu H. Sonochemical synthesis of highly photoluminescent carbon nanodots. RSC Adv. 2014 Oct 16;4(94):52230–4.

189.   Kumar VB, Porat Z, Gedanken A. Facile one-step sonochemical synthesis of ultrafine and stable fluorescent C-dots. Ultrason Sonochem. 2016 Jan;28:367–75.

190.   Xu X, Ray R, Gu Y, Ploehn HJ, Gearheart L, Raker K, et al. Electrophoretic Analysis and Purification of Fluorescent Single-Walled Carbon Nanotube Fragments. J Am Chem Soc. 2004 Oct 1;126(40):12736–7.

191.   Bottini M, Balasubramanian C, Dawson MI, Bergamaschi A, Bellucci S, Mustelin T. Isolation and characterization of fluorescent nanoparticles from pristine and oxidized electric arc-produced single-walled carbon nanotubes. J Phys Chem B. 2006 Jan 19;110(2):831–6.

192.   Liu H, Ye T, Mao C. Fluorescent Carbon Nanoparticles Derived from Candle Soot. Angew Chem Int Ed. 2007;46(34):6473–5.

193.   Zhao Q-L, Zhang Z-L, Huang B-H, Peng J, Zhang M, Pang D-W. Facile preparation of low cytotoxicity fluorescent carbon nanocrystals by electrooxidation of graphite. Chem Commun. 2008 Oct 27;(41):5116–8.

194.   Yao S, Hu Y, Li G. A one-step sonoelectrochemical preparation method of pure blue fluorescent carbon nanoparticles under a high intensity electric field. Carbon. 2014;C(66):77–83.

195.   Bourlinos AB, Stassinopoulos A, Anglos D, Zboril R, Georgakilas V, Giannelis EP. Photoluminescent Carbogenic Dots. Chem Mater. 2008 Jul 1;20(14):4539–41.

196.   Wang F, Pang S, Wang L, Li Q, Kreiter M, Liu C. One-Step Synthesis of Highly Luminescent Carbon Dots in Noncoordinating Solvents. Chem Mater. 2010 Aug 24;22(16):4528–30.

197.   Krysmann MJ, Kelarakis A, Dallas P, Giannelis EP. Formation mechanism of carbogenic nanoparticles with dual photoluminescence emission. J Am Chem Soc. 2012 Jan 18;134(2):747–50.

198.   Zheng M, Xie Z, Qu D, Li D, Du P, Jing X, et al. On-off-on fluorescent carbon dot nanosensor for recognition of chromium(VI) and ascorbic acid based on the inner filter effect. ACS Appl Mater Interfaces. 2013 Dec 26;5(24):13242–7.

199.   Liu R, Wu D, Liu S, Koynov K, Knoll W, Li Q. An aqueous route to multicolor photoluminescent carbon dots using silica spheres as carriers. Angew Chem Int Ed Engl. 2009;48(25):4598–601.

200.   Zhu H, Wang X, Li Y, Wang Z, Yang F, Yang X. Microwave synthesis of fluorescent carbon nanoparticles with electrochemiluminescence properties. Chem Commun. 2009 Sep 14;(34):5118–20.

201.   Wei W, Xu C, Wu L, Wang J, Ren J, Qu X. Non-Enzymatic-Browning-Reaction: A Versatile Route for Production of Nitrogen-Doped Carbon Dots with Tunable Multicolor Luminescent Display. Sci Rep. 2014 Jan 6;4(1):3564.

202.   Guan W, Gu W, Ye L, Guo C, Su S, Xu P, et al. Microwave-assisted polyol synthesis of carbon nitride dots from folic acid for cell imaging. Int J Nanomedicine. 2014 Oct 31;9(1):5071–8.

203.   Zhu S, Meng Q, Wang L, Zhang J, Song Y, Jin H, et al. Highly Photoluminescent Carbon Dots for Multicolor Patterning, Sensors, and Bioimaging. Angew Chem Int Ed. 2013;52(14):3953–7.

204.   Dong Y, Pang H, Yang HB, Guo C, Shao J, Chi Y, et al. Carbon-based dots co-doped with nitrogen and sulfur for high quantum yield and excitation-independent emission. Angew Chem Int Ed Engl. 2013 Jul 22;52(30):7800–4.

205.   Guo Y, Wang Z, Shao H, Jiang X. Hydrothermal synthesis of highly fluorescent carbon nanoparticles from sodium citrate and their use for the detection of mercury ions. Carbon. 2013 Feb;52:583–9.

206.   Qu D, Zheng M, Zhang L, Zhao H, Xie Z, Jing X, et al. Formation mechanism and optimization of highly luminescent N-doped graphene quantum dots. Sci Rep. 2014 Jun 18;4(1):5294.

207.   Bhunia SK, Saha A, Maity AR, Ray SC, Jana NR. Carbon Nanoparticle-based Fluorescent Bioimaging Probes. Sci Rep. 2013 Mar 18;3(1):1473.

208.   Fang Y, Guo S, Li D, Zhu C, Ren W, Dong S, et al. Easy synthesis and imaging applications of cross-linked green fluorescent hollow carbon nanoparticles. ACS Nano. 2012 Jan 24;6(1):400–9.

209.   Jiang H, Chen F, Lagally MG, Denes FS. New Strategy for Synthesis and Functionalization of Carbon Nanoparticles. Langmuir. 2010 Feb 2;26(3):1991–5.

210.   Zhuo Y, Miao H, Zhong D, Zhu S, Yang X. One-step synthesis of high quantum-yield and excitation-independent emission carbon dots for cell imaging. Mater Lett. 2015 Jan 15;139:197–200.

211.   Lai C-W, Hsiao Y-H, Peng Y-K, Chou P-T. Facile synthesis of highly emissive carbon dots from pyrolysis of glycerol; gram scale production of carbon dots/mSiO2 for cell imaging and drug release. J Mater Chem. 2012 Jul 3;22(29):14403–9.

212.   Kwon W, Rhee S-W. Facile synthesis of graphitic carbon quantum dots with size tunability and uniformity using reverse micelles. Chem Commun. 2012 May 2;48(43):5256–8.